Reproduction of Hierarchically Rough Surfaces via Micromolding Surface-Initiated Polymerization

By

Jarrid Scott Ristau

Thesis

Submitted to the Faculty of the

Graduate School of Vanderbilt University

in partial fulfillment of the requirements

for the degree of

MASTER OF SCIENCE

in

Chemical Engineering

December 2014

Nashville, Tennessee

Approved:

G. Kane Jennings, Ph.D.

Scott Guelcher, Ph.D.

For Allison

Table of Contents

List of Figures

List of Schemes

List of Tables

Acknowledgements

While composing this thesis has been a challenging task, it could never have come to pass without the people who have cared for me in ways I am still only beginning to appreciate. The wisdom and generosity of the men and women who have helped me along my path are humbling. I have dedicated this work to my stepmother, Allison Ristau, because her loving support has been a constant force since the day she became a part of my family. I am further blessed to have parents – Scott Ristau and Teri Unterreiner – who have put my wellbeing and education ahead of everything else, and who have made great sacrifices so that I never had to.

As for my education, I am indebted to Vanderbilt University and the many faculty who make this proud institution what it is. I would like to thank Kane Jennings for becoming my advisor, but also for inspiring me to stay excited about our field. It was in his fluid mechanics lecture where I saw the continuity equation derived from a shell balance, and that moment will live in my memory as one of the first times that mathematics (and more importantly, its value) resonated deeply with me. Dr. Jennings ignited my interest in surface phenomena in another course, and through work on one of its project, I came to be involved with original research in his lab. I owe a great deal also to Carlos Escobar, who taught me everything I know about surface modification in practice and who originally developed the technique used in this work.

Vanderbilt is a community, and I must also mention many others without the assistance of whom this work would have been impossible. I would like to thank Russell Dunn for his unwavering support and advocacy on my behalf. I would like to thank Paul Laibinis for his initial access to equipment and resources in the infancy of this project, and for his generosity and effectiveness as a professor. Additionally, I am grateful to Scott Guelcher who, as my

undergraduate advisor, offered advice in my first weeks at Vanderbilt that got me ahead in my studies and made possible the completion of this masters work.

Finally, I would like to thank the National Science Foundation for offering financial support through the grant CBET-1134509.

Abstract

Micromolding surface-initiated polymerization (μMSIP) – a recent addition to the soft lithographic toolbox – represents a unique and powerful approach in surface fabrication. As the name suggests, this technique marries two techniques; micromolding is used to generate casts of a substrate of interest and surface-initiated polymerization (SIP) follows for reproduction of the surface architecture with a covalently bound polymer thin film. Importantly, a number of SIP approaches employ partially fluorinated materials thereby offering a route to ultralow energy surfaces with desirable properties. Previous work with this technique has been restricted to bioinspired surfaces, such as plant leaves and to several machined surfaces that were useful in assessing polymerization kinetics. The focus of this work has been extending μMSIP to new and more challenging surfaces. Novel surfaces of various types have been fabricated as substrates for molding and reproduced. Smaller feature sizes, including both micro- and nanoscale roughness, have been shown beyond those previously demonstrated. Additionally, replication of re-entrant surface geometry – indispensable for superomniphobicity – has also been achieved. Many of these films demonstrate superhydrophobicity, and some have proven superoleophobic as well. The development and expansion of μMSIP will prove invaluable not only for its many applications and unique properties, but also because it enables researchers to characterize many surfaces that would be impossible to generate with other techniques. Such research may open the door to great extensions in our understanding of the many phenomena at the surface.

1 Background

1.1 Surface Properties

1.1.1 Preface

We speak often of "the surface of things" with dismissiveness. It is not the locale of substance, but rather of incompleteness. However, the extension of this social axiom into scientific pursuits would prove an insidious thing. In nature, surfaces defy expectation. Surfaces break continuums; they riddle mathematical models with infinities and other failings. Yet, they are a comfortable reality. We interact intimately with them, convincing ourselves that what matters is on the inside. In fact, it is the surface of things that we have only begun to see.

Italo Calvino challenged traditional perspective in his work *Palomar*, writing "Only after knowing the surface of things can one throw himself into the search for what is underneath. But the surface of things is endless." The underlying message of the passage applies equally well to scientific investigation as it does to literature, but the reason is somewhat distinct. As our knowledge of science expands, we have largely reconciled the phenomena characteristic of a material's bulk phase. It is at the surface where our models fall short.

The fact that interfacial processes remain poorly understood has to do with several realities. Interfacial phenomena have an extreme sensitivity to contaminants and physical modification. Therefore, the success of studying these regions has been contingent on the development of precise control and analysis for experiments – vacuum conditions, clean rooms, selection of idealized surfaces (e.g. gold), and even an understanding of crystallography and adsorption. Additionally, of course, the nature of a surface is only clear at incredibly small scales

– the micro- and nanoscale – and probing them was nearly an impossibility before the development of electron microscopy.

That same advancement however led to another of the major problems yet to be resolved. While the solid-vacuum interface may be readily probed, the solid-liquid interface cannot. Electron beams become inapplicable with fluid present, and while we may gain an understanding of a solid surface, we cannot yet directly probe these surfaces when they are in contact with a liquid. Understanding how these surfaces change under such circumstances is one of the fundamental questions of this field.

Finally, the advancement of this field has been halted not only for technological reasons, but also as a consequence of the mathematical shortcomings. Some of the basic problems of capillarity are only now beginning to be solved – 180 years after Young and Laplace introduced them. Contact angle hysteresis and the transition from complete to partial wetting represent a few of these obstacles.

As an engineer, it is prudent to consider the applications of research before ascribing it value; however, the importance of developing our grasp of surface phenomena should be self-evident. Many practical processes involve the spreading of a liquid on a solid, and control over surface properties offer a designer a means to control the properties of a material by modifying its surface selectively. That is, a bulk material can be made to have different properties without changing the bulk material altogether. This is perhaps most familiar to us in the kitchen, where non-stick coatings have allowed chefs to enjoy the indispensable properties of metal cookware – their ability to transfer heat readily and efficiently – while mitigating one of the drawbacks – that food sticks to the pan. These best-of-both-worlds scenarios are innumerable and offer design benefits at virtually any scale. From developing pipes that resist corrosion in chemical plants to

manufacturing self-cleaning windows, which could simplify the cleaning schedule of a homeowner, keep automobile drivers safer by minimizing obstruction to their field of vision, or eliminate hundreds of dangerous man-hours spent maintaining sparkling clean windows of skyscrapers in our cities.

1.1.2 The origin of surface properties

Surface properties arise due to the unfavorable balance of forces experienced by material at an interface. Attractive forces between molecules (which are responsible for the existence of the liquid state) are known to subject molecules in the interior of a liquid to equal forces in all directions. At the surface, contrarily, the molecules experience a net inward pull due to the imbalance of forces. This can be seen in Figure 1 below. As a consequence of this imbalance, molecules at the surface of a liquid tend to move toward the interior resulting in the spontaneous contraction of the surface. It is because of this that liquid droplets and vapor bubbles tend to attain a spherical shape at equilibrium. A sphere can be demonstrated to have the lowest surface area to volume ratio, and therefore – for a given number of molecules – a spherical geometry represents the case with the maximum number of molecules in the interior and the minimum at the surface[1].

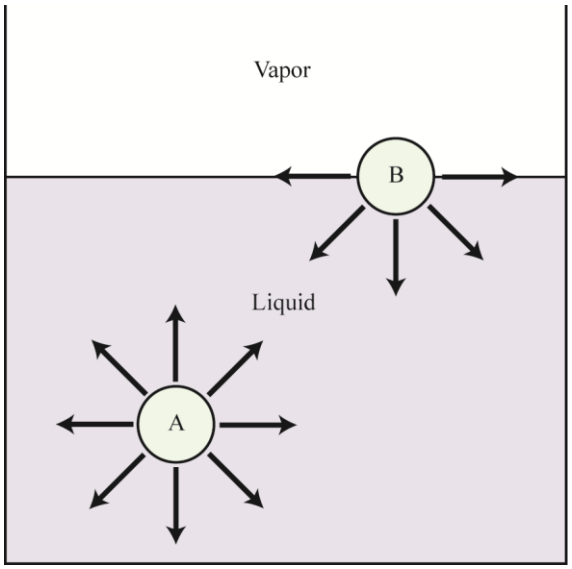

Figure 1 Intermolecular forces in the bulk liquid phase exhibit approximately equal magnitudes in all directions (molecule A). At the surface, an imbalance of these forces exists, resulting in the net movement of surface molecules toward the interior (molecule B).

It is worth noting that these properties are typically restricted to solid-vapor, solid-liquid, liquid-vapor, and $liquid_1$-$liquid_2$ interfaces. At solid-solid interfaces, the bonding and molecular structure limit the potential for surface molecules to reorient, and vapor-vapor interfaces are prevented from forming because of the ease with which gas molecules mix.

1.1.3 Wetting, Spreading, & Contact Angle

Wetting of a surface involves the displacement of one fluid by another, and therefore it generally involves three phases – the solid surface and at least two fluids, most commonly a liquid and a vapor. For the situation in which a liquid wets a solid surface by displacing a gas, there exist three distinct categories of wetting phenomena:

1. Spreading wetting
2. Adhesional wetting

3. Immersional wetting

In the case of spreading wetting, the most familiar of the three, a liquid in contact with a solid surface spreads over it so as to increase the increase the solid-liquid and the liquid-vapor interfacial areas and to decrease that of the solid-vapor interface. Whether spreading will occur spontaneously may be determined using the spreading coefficient (S) which may be defined as

$$S = \frac{-\Delta G_s}{A} = \gamma_{SV} - (\gamma_{SL} + \gamma_{LV})$$

where ΔG_s is the increase in free energy due to spreading. A liquid will spread spontaneously when $S \geq 0$. When the spreading coefficient is negative, the liquid exists as a droplet on the surface having a finite contact angle (Θ). Such a case is referred to as partial wetting, and complete wetting occurs when the contact angle equals zero[2].

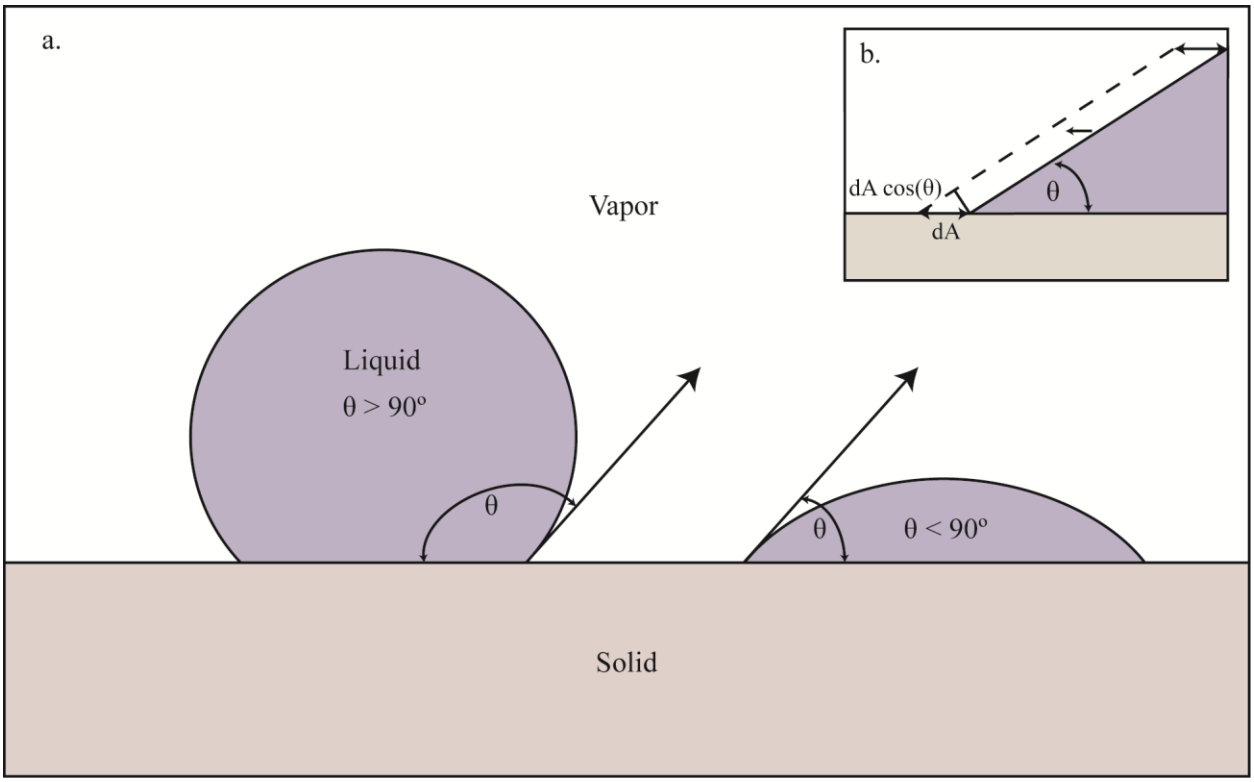

Figure 2 The equilibrium contact angle is determined by far-field thermodynamic parameters (i.e. the interfacial energies per unit area of each interface). It may be predicted using Young's Equation, which is derived for a wedge as shown in b.

The equilibrium contact angle (Θ_e) occurs for a system when the total surface free energy of a system (i.e. $\gamma_{SV}A_{SV} + \gamma_{SL}A_{SL} + \gamma_{LV}A_{LV}$, where A represents the interfacial area) is at a minimum. For the case of a liquid spreading over a solid, as shown in Figure 2, one finds that as the solid-liquid interface increases by an infinitesimal amount (dA), the increase in liquid-vapor interfacial area may be shown to be $dA\ cos(\Theta)$. Consequently, the increase in free energy (dG) is given by

$$dG = \gamma_{SL}dA + \gamma_{LV}\ dA\ cos(\Theta) - \gamma_{SV}dA$$

When the system is at equilibrium, $dG = 0$, and the equation may be reduced to

$$\gamma_{SL} + \gamma_{LV}\, cos(\Theta_e) - \gamma_{SV} = 0$$

This equation, derived for a wedge, is known as Young's equation, and can be rearranged to the form

$$\cos(\Theta_e) = \frac{\gamma_{SV} - \gamma_{SL}}{\gamma_{LV}}$$

The utility of this equation is significant. However, because it is derived for a wedge, many applications require the superimposition of some curvature. Additionally, for the special case where $\gamma = \gamma_{SV} - \gamma_{SL}$, $\cos(\Theta_e) = 1$, and $\Theta_e = 0$. This represents complete wetting of the surface[2].

The line that delimits the wetted area of the surface is called the contact line ($\mathcal{L}$), and for droplets, it takes the shape of a circle. Three phases exist in contact at the contact line, the solid, liquid, and equilibrium vapor, and each of the interfaces has an interfacial free energy per unit area associate with it (i.e. γ_{SL}, γ_{SV}, and γ_{LV}. Each of these parameters describes "far-field" (that is, far from $\mathcal{L}$) adequately; however, in the region of the contact line the situation becomes dramatically more complex and requires detailed knowledge of the system. With his equation, British scientist Thomas Young successfully related the equilibrium contact angle to these far-field energies using a derivation that requires no knowledge of the materials' core. The usefulness of this is clear, as θ_e is entirely defined by thermodynamic parameters. The measured contact angle can therefore provide information on the interfacial energies of a system. Because $\gamma_{LV} = \gamma$, which is known for most liquids, the contact angle can be used to calculate the difference $\gamma_{SL} - \gamma_{LV}$.

1.1.4 Advancing and Receding Contact Angle

While the equilibrium contact angle has tremendous value, it also comes with certain limitations inherent to the approach. Because it uses far field thermodynamic parameters rather than detailed information about the region near the contact line, it is typically used only as an estimate. For one thing, a liquid behaves differently when it spreads over a solid surface compared to when it contracts away during dewetting. Consequently, different contact angles are generally measured for these values. The advancing contact angle (θ_a) is measured when the solid-liquid contact area is increasing, and the receding contact angle (θ_r) is measured when the solid-liquid contact area is decreasing. The equilibrium contact angle generally falls somewhere between these two values.

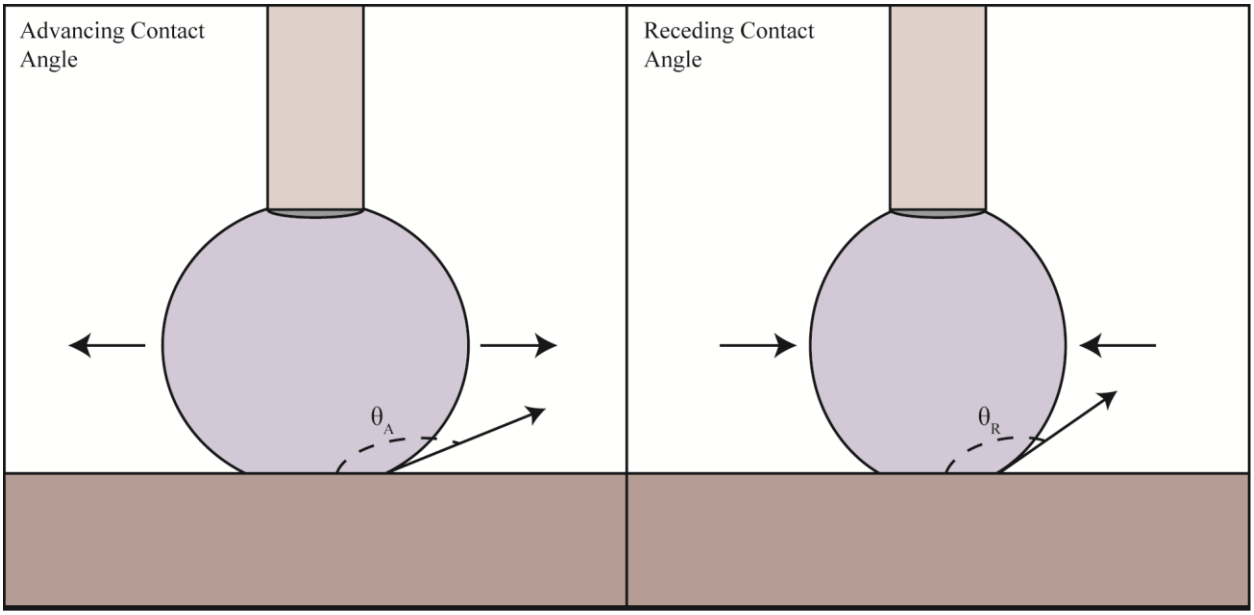

Figure 3 The advancing contact angle (left) is measured as the solid-liquid interfacial area increases and the receding contact angle is measured as that interfacial area decreases (right).

1.2 Fluorine and its Polymers

Few synthetic polymers have become as familiar as Teflon, and for good reason. Non-stick pans are a star in the kitchen – among the greatest things since sliced bread – and Teflon's star-power was cemented when NASA began using it for space travel, using the polymer in heat shields, cargo hold liners, and space suits. In fact, the thrust to celebrity generated by NASA earned Teflon a spot as one of the spin-off inventions commonly used to justify the public value of a space program – right next to Velcro and Tang. And just like Velcro and Tang, NASA did not invent Teflon either.

Teflon is the trade name for polytetrafluoroethylene (PTFE), a substance first synthesized by DuPont in 1938. As with many great feats of scientific discovery, PTFE emerged by happy accident when Roy Plunkett was using tetrafluoroethylene (TFE) as an intermediate in producing a Freon compound. This new compound was found to have excellent acid and corrosion resistance; it remained solid and stable at higher temperatures than any polymer known at the time; and it did not melt like other plastics. In addition to its more glamorous use by NASA, Teflon was used heavily by American forces in the Second World War before ultimately becoming one of DuPont's most profitable products[3].

The accolades, however, should come as no surprise. Fluoropolymers have a number of unique properties as a consequence of fluorine's special place on the periodic table. Fluorine is the most electronegative element and forms extremely strong bonds as a result. It can readily replace hydrogen in many organic molecules and, when incorporated, confers myriad (and often contradictory) properties onto the system. For instance, inclusion of fluorine can result either in increased polarity or in decreased polarity, in improved chemical reactivity or in near-complete

inertness. A neutral polyolefin film, when slightly fluorinated becomes suddenly polar, and this is a common technique for making polyolefin surfaces adhereable. However, as the fluorine content is increased, the film becomes completely neutral. The relationship between increasing fluorine content and a number of important properties are summarized in the Table 1 below[4].

Table 1 Effect of increasing fluorine content on polymer properties

Property	Impact
Chemical resistance	Increases
Melting point	Increases
Coefficient of friction	Decreases
Thermal stability	Increases
Dielectric constant	Decreases
Dissipation factor	Decreases
Volume and surface resistivity	Increase
Mechanical properties	Decrease
Flame resistance	Increases
Resistance to weathering	Increases

Fluoropolymers became so pervasive because of these desirable (and in many cases, unparalleled) characteristics. They have the lowest critical surface energy of known materials, resulting in exceptional lubrication properties. Their low dielectric constants and melting points (both lower than polyethylene) make them a superior choice for insulator applications, such as in cables or circuit boards. Their chemical inertness is invaluable in terms of polymer stability, but more subtle advantages exist as well. For instance, PTFE cannot be cross-linked, making it susceptible to creep. Nevertheless, often used for seals, this is beneficial because it enables improved conformal contact with the surface.

On a given day, each of us encounters more fluoropolymers that we can likely imagine, a point well illustrated by Ebnesajjad in the first chapter of his handbook. Walking through a

typical family routine, one would be hard pressed to notice even half of the fluorocompounds encountered in a day. Hardly just for non-stick pans, PTFE strips may be found on your razor as a safety measure. Many electronic components – coaxial cables, for example – use fluoropolymer insulation for the low dielectric constant. Even your doctor is feeding you fluorinated compounds – 25% of all marketed drugs contain fluorine, including three of the top ten sellers in 2011. Fluorine-containing pharmaceuticals exhibit improved potency and selectivity, offer enhanced tissue penetration and drug half-life, and show fewer drug interactions. The inner metal surface of your son's asthma inhaler is coated with a fluoropolymer that prevents drug adhesion, and another fluorocompound ensures delivery of the prescribed amount. Grandma, who recently got herself some new arteries in a vascular grafting surgery now has blood pumping through tubes expanded polytetrafluoroethylene (ePTFE), and the anesthetic that made the surgery possible was a fluorocarbon gas.

Thinking green, polyvinyl fluoride (PVF) represents a component of photovoltaic cells, protecting against oxidation and corrosion and improving the cell's lifetime. Fluoropolymer-coated bags are used by coal plants to reduce particulate emissions, and power plants employ a variety of fluorocarbon species to mitigate greenhouse gas release. Polyvinylidene difluoride (PVDF) is included as an additive in exterior paints for combatting combat weathering, upping their expected life to at least thirty years. Polyvinyl fluoride (PVF) is a robust coating used in airplane cabin interiors to resist fire and harsh cleaning. Fluorinated compounds have even made it beyond the atmosphere and potentially out of the solar system as well. There are almost certainly Teflon components continuing their decades-long mission aboard Voyager 1.

The applications – with little exaggeration – continue ad infinitum. Although the above may have seemed a tedious exercise, the unrivaled potential for these compounds is almost indisputable.

1.3 Environment, Health, and Safety

Despite their appeal, concerns regarding the safety and environmental impact of fluorocompounds have been raised in the recent decades. Environmental concerns about the ozone layer (whose thinning was due in large part to chlorofluorocarbons), leakage of refrigerants (which are almost all fluorocarbon based), and fluorocarbon emissions (they are, themselves, greenhouse gases) have all brought these stars of polymer science under scrutiny. Additionally, although PTFE is one of the most inert compounds known, its monomer – tetrafluoroethylene, a gas – is an exceptionally volatile explosive. Production of PTFE is a dangerous game, and considering the amount produced annually, safer alternatives would be desirable.

Production concerns do not end with the dicey conditions of the gas-phase polymerization. The processability is of fluoropolymers abysmal. Fluoropolymers are typically applied by spin-coating or dip-coating (which are only possible on planar surfaces and rely on physical adherence, lacking direct attachment to the substrate), by solution casting, or by chemical adsorption, which yields only low density polymer due to steric and diffusional limitations[5]. As a result of these mounting concerns, alternatives have become a hot area of research.

1.4 Surface-Initiated Polymerization

Since the advent of Grubbs catalyst, a new possibility has emerged. Instead of polymerization in the gas phase, consider the possibility of covalently attaching many single active mers to a surface. If this surface is then placed in solution, it follows that chain growth will proceed from these termini, resulting in a polymer film directly attached to that surface. This is the essence of a remarkable technique known as surface-initiated polymerization (SIP). This approach has the benefits of providing robust attachment to the surface, being far less limited in the geometries to which it may be applied, and the possibility of highly controllable growth. However, to date, SIP films containing fluorine have been primarily generated with post-processing. For example, poly(hydroxyethyl methacrylate) (PHEMA) films have been growth using SIP and then subsequently modified with perfluoro- acid chlorides[6]. However, almost no examples can be found of partially fluorinated films grown directly using SIP. Ruhe et al is one exception, using controlled radical polymerization; however the polymerization time is long 4 and 27 hours to produce only very thin films (20 and 70 nm)[7,8].

Furthermore, the concerns about health and safety mentioned above are largely in regard to perfluorinated compounds, and one of the ways those problems have been addressed is use of only partially-fluorinated polymers wherever possible. They offer great advantage, both for safety and processability, and have shown themselves to be safer, less expensive, and simpler to produce[5]. However, the examples of SIP in the literature that use such fluoromonomers are still more limited.

Fortunately, the monomer which is at this point best suited to SIP is partially fluorinated – the family of the 5-(perfluoro-*n*-alkyl)norbornenes. Norbornenes are a well-studied family of

compounds that undergo ring-opening metathesis polymerization (ROMP) under mild reaction conditions. This family has a high reactivity, and is easily synthesized – and even functionalized. This monomer, therefore, offers some hope, with the combination of the surface-initiation strategy and ROMP, surface-initiated ring-opening metathesis polymerization (SI-ROMP) was introduced as a viable technique for producing partially fluorinated thin films[5].

1.5 SI-ROMP of NBFn: Process Overview

Considering the remarkable properties conferred to these films by the fluorocarbon moieties, the conceptual simplicity is exciting. The guiding principle is that polymerization of monomers in solution is initiated by a catalyst-activated monomer, which has been chemically bound to the surface. The procedure is outlined in Scheme 1 below.

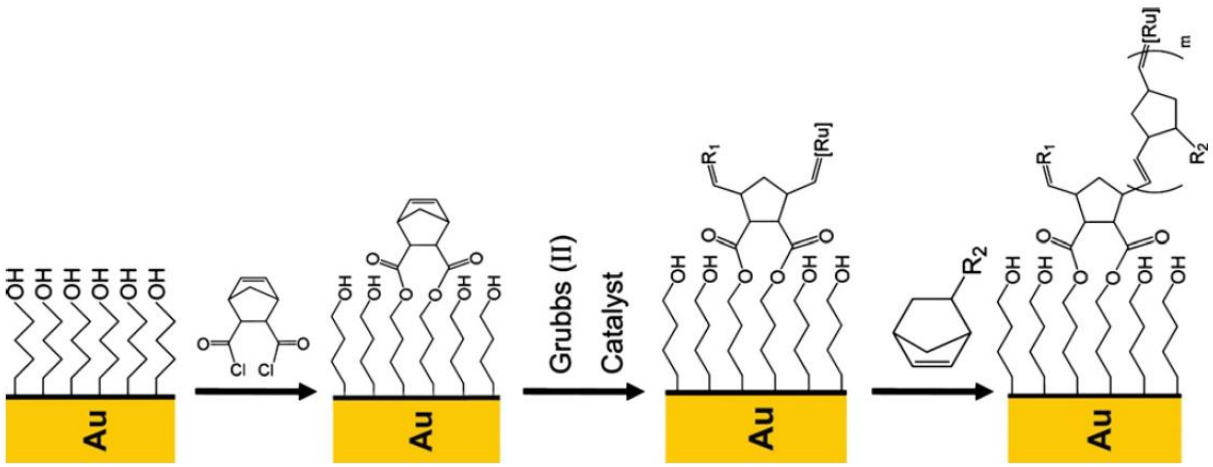

Scheme 1 Surface-Initiated Ring Opening Metathesis Polymerization of NBFn. A hydroxyl-terminated self-assembled monolayer (SAM) is formed on gold by treatment with mercaptobutanol, and the subsequently modified by exposure to 5 mM trans-5-norbornene-2,3-dicarbonyl chloride for 30 min. Grubbs Catalyst (2nd Gen.) then activates the surface-bound norbornene, which is ultimately exposed to a solution of the fluoronorbornene monomer resulting in polymerization

Chemical attachment of the initiator to the surface is achieved in two steps. First, a planar gold surface (formed by evaporation of 99.99% gold shot onto a silicon wafer) is exposed to a 1 mM solution of mercaptobutanol in ethanol for 1 hour. The adsorption of n-alkanethiols onto gold has been heavily investigated since its famed discovery, and although gold is typically considered inert, thiols bind well and rapidly (~ 1 h). This enables functionalization of the gold surface, because the self-assembled monolayer (SAM) will orient such that the terminal group opposite the thiol is exposed. With mercaptobutanol, the gold surface achieves nearly complete monolayer coverage, resulting in abundant hydroxyl groups at the interface and enabling further modification[5].

Next, the modified gold surface is exposed to the initiator molecule solution of 5 mM trans-5-norbornene-2,3-dicarbonyl chloride in dichloromethane (DCM) for 30 min. This di-acid chloride reacts with the exposed hydroxyl group, forming an ester attachment and resulting in a norbornenyl-decorated surface. The surface-tethered initiator is activated in the third step by exposure to 5 mM Grubbs Catalyst 2nd Gen. ((1,3-Bis-(2,4,6-trimethylphenyl)-2-(imidazolidinylidene) (dichlorophenylmethylene) (tricyclohexylphosphine) ruthenium) in DCM for 10 minutes, and the resulting surface is active for ROMP. The surface is then quickly (but thoroughly) washed with DCM, and finally immersed in a monomer solution in DCM ranging from 0.005 M to 1.0 M NBFn. Polymerization time may range from 1 to 15 minutes, and the film thickness increases with time. Above 15 minutes, coupling and backbiting reactions prevent further growth of the film and can even result in decreased film thickness[5] Furthermore, there is great opportunity for expansion and optimization. It has been shown that one strategy for kinetic improvements is growth first of a macroinitiator (PHEMA) from the surface by ATRP, which is then followed by SI-ROMP of the fluoronorbornenes.

A critical consideration in implementation of novel coatings is the ability to tailor surface properties to the application. One of the most significant features one hopes to control is the thickness of the film. Our group demonstrated that film thickness of the PNBFn by SI-ROMP increases with increasing fluoropolymer chain length (n), which may be seen in Table 2 below.

Table 2 Film thickness and impedance properties of PNB and PNBFn polymers as a function of chain length (n)

film	thickness (nm)	$\log(R_f(\Omega\ cm^2))$	C_f (nF/cm^2)
initiator		1.3	19 000
pNB	49	4.3	250
pNBF4	52	6.2	63.2
pNBF6	612	6.4	4.6
pNBF8	713	7.4	2.8
pNBF10	1565	7.5	1.6

Interestingly, our group previously showed precisely opposite effect when exploring SI-ROMP of polynorbornenes (PNBHn) bearing only an alkyl chain (in contrast with a fluoroalkyl chain)[9]. For PNBHn polymers, increasing chain length leads to undesirable effects including thinner films, more defects, and formation of only sparse polymer islands when n approaches 10.

This contrast offers insight into the mechanism underlying the process. It has been suggested that chain folding accounts for the contradictory trends of PNBFn and PNBHn. It is likely that longer fluorocarbon chains elevate the norbornene ring strain, due to their electron-withdrawing character. Because ring strain is the driving force for ROMP, it follows that more highly strained rings should polymerize more readily[5]. This can account, very generally, for the improved reactivity of the NBFn monomers for SI-ROMP, but is not the end of the story.

An important observation here is that the film thicknesses of PNBFn and PNB (n = 0) are comparable when n = 4 (~50 nm), but when the chain length is increased to six, the thickness of PNBFn jumps an order of magnitude whereas the thickness of PNBHn films is diminished[5,9]. It was noted by Perez et al in their description of the monomer synthesis that for the endo conformation (which dominates, comprising 80% of the products) the fluorocarbon chains tend to fold in toward the olefin, which is expected to obstruct access the ring and inhibit ROMP[10]. Furthermore, it is well established that long fluorocarbon chains are much stiffer than their equivalent-length alkane, and therefore one expects this folding to be diminished at longer chain lengths. Indeed, Perez et al showed that for $n \geq 6$, the fluorocarbon's ability to fold shows a marked decline, and this effect was attributed to the chain rigidity[10]. Long alkyl chains, on the other hand, have much greater conformational freedom, and their capacity for folding ought not to be reduced for larger n.

With this in mind, all of the above observations regarding film thickness and chain length – for both species – may be explained on at least a qualitative level. When n = 4, both the fluorinated and the alkyl chains may fold, causing steric hindrance and reducing the monomers' activity for ROMP. For longer chain lengths, the increased stiffness of the fluoroalkyl substituent causes a reduction in folding, and this in turn makes the norbornene ring more accessible for ROMP. This accounts for the significant jump in thickness of PNBFn where n = 6, as well as for the continued improvement in reactivity of NBFn with longer (and stiffer) chains. Contrarily, long alkyl chains will not exhibit the same folding reduction, and partitioning towards the ring is likely greater when n is increased. As a result, PNBHn show reduced reactivity for longer chains because, when folded, the longer chain will occupy a greater volume than a shorter one, limiting access to the ring to more completely.

This explanation is a satisfying one, but more importantly, it is a compelling example how subtle nuances of fluoropolymers may be used to great benefit. These sorts of multifaceted behaviors, while initially a challenge to rationalize, are the very same details that permit elaborate feats in materials engineering if properly understood

After exploring the effect of chain length on film thickness as described above, our group employed electrochemical impedance spectroscopy (EIS) to demonstrate why exactly one might hope to understand and control properties such as film thickness. EIS is used to characterize the opposition of alternating current (AC) flow at a complex interface, and it efficiently captures energy storage and dissipation characteristics as well as quantifying a protective coating's resistance to the diffusion of ions. It was found that impedance scales with film thickness of PNBFn at all AC frequencies. This is significant because it suggests thicker films provide a more robust barrier with fewer defects, and this is manifest by reduced penetration of the redox probes[5]. In this testing, $K_3Fe(CN)_6$ and $K_4Fe(CN)_6$ were chosen as redox probes with Na_2SO_4 (0.1 M) supporting electrolyte. When fit with Randall's equivalent circuit and a Warburg impedance term (to capture mass transfer), the resistances and capacitances for the film have values similar to those of other fluorinated films known to provide an outstanding barrier[6]. These results suggest that PNBFn films grown by SIP have good potential as protective coatings and would exhibit excellent corrosion resistance.

1.6 Micromolding Surface-Initiated Polymerization

Imbuing an ordinary surface with texture at the micro- and nanoscales has been shown to have many applications in fields including microelectronics[11], optics[12], drag reduction[13], and corrosion resistance[14]. Micromolding surface-initiated polymerization (μMSIP) has been added

to the soft lithographic toolbox recently. At its core, μMSIP depends on the marriage of two distinctly defined techniques. Micromolding (μM) is employed to form a negative replica of a surface of interest, and surface-initiated polymerization (SIP) is used to reproduce that surface architecture by polymerization of monomer filling the mold. Catalysis is achieved when the prepolymer-filled mold is brought into contact with the active surface. The process is outlined in Scheme 1 below.

Micromolding surface-initiated polymerization offers several advantages[15]. First, it enables the engineer to create surface-bound polymer coatings, setting itself apart from virtually all other soft lithographic techniques where the features are restricted to physisorption, hampering long-term stability of the coatings[16]. Films generated by μMSIP are chemically bound to the surface by covalent bonds, substantially improving their robustness. Equally importantly, μMSIP has been demonstrated for polymerizations that offer a relatively simple route to fabricating partially fluorinated polymer films. Partially fluorinated polymers are desirable for numerous reasons outlined previously. Third, it has been shown that μMSIP allows the engineer control over the feature height on the final polymer film by tuning the catalyst concentration and temperature to produce the desired result. Feature heights ranging from 20% - 100% of the original mold were demonstrated[15].

At its simplest, μMSIP involves the following steps. First, a surface is selected with an architecture of interest for reproduction as a polymer film. This surface is termed the "master", and a negative cast of the surface is generated in the second step – micromolding. A soft polymeric material (almost ubiquitously PDMS, though alternatives exist) is poured over the surface as a viscous fluid which fills the voids around any surface features. The polymer is then cured, resulting in a solid mold bearing the negative image of the master surface. This mold is

then peeled from the master, and the master can be cleaned and used to create another mold. Next, a particular polymerization chemistry feasible for SIP is selected; the mold filled with monomer; and the desired substrate activated to initiate polymerization. Finally, the active surface is brought into contact with the pre-polymer filled mold, and the polymerization reaction proceeds resulting in a surface-bound polymer film with the architecture of the master surface.

Scheme 1 addresses the particular case of a master surface covered with a grid of microscale pyramids. The surface is cast in a composite mold comprised of a hard PDMS layer and a Sylgard 184 PDMS layer. The mold is peeled off, and initiator for the polymerization reaction is added to the mold's recesses, facilitating 100% reproduction of the mold's feature height. The active surface is prepared and the mold filled with monomer. The surface is then pressed onto the mold as quickly as possible to begin polymerization from the surface. Once the polymerization is complete, the pyramidal surface is reproduced as a polymer film.

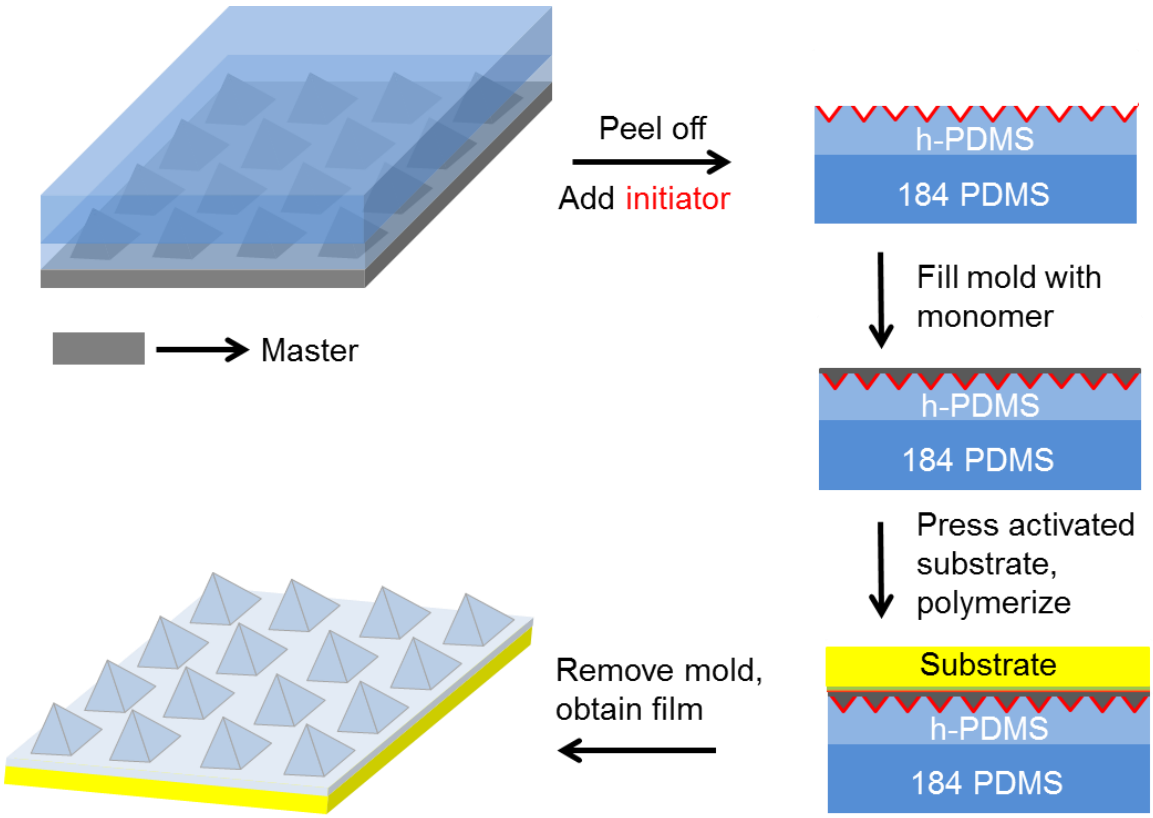

Scheme 2 The μMSIP process used to produce microtextured PNBF8 films. Initiator is not added if the surface features are desired to be smaller than the master features[15].

Four primary surface architectures have been reproduced in previous work, including diamond field emitter arrays (DFEA), Klarite, and the leaves of two superhydrophobic plants, *Trifolium repens* and *Aristolochia esperanzae*. The former two substrates were chosen because their precise geometry was ideal for preliminary characterization of the new technique – particularly with AFM. The ability to assess feature height accurately was critical in demonstrating the tunable feature height as well as evaluating the polymerization kinetics. The latter two master substrates were chosen in part because of their superhydrophobicity, but also because of the historical roots of this field to biological surfaces - with almost all research

interest in this field stemming at some point from the "lotus effect". These two plant leaves were readily available and showed the same properties that sparked the interest in the lotus leaf.

Several aspects of the polymerization were optimized, and one factor that was found to be critical was the initiation approach. It was found that SI-ROMP initiated solely by surface bound catalyst, was inadequate for achieving 100% of the feature heights of the mold. Two approaches were investigated as alternatives to the monolayer initiated approach. A macroinitiation method was tested where a layer of pHEMA was first bound to the gold substrate (via SI-ATRP) to increase the available surface area for catalyst binding. With more catalyst on the surface, greater polymerization conversions are possible, enabling larger features to be grown. It was also shown that initiator added directly to the mold prior to the prepolymer offers the most promising results, with a shorter polymerization time able to achieve larger feature heights and conversions approaching unity.

A comparison of the three approaches can be seen in Figure 4 below. The macroinitiation approach outperforms the monolayer initiated approach, as expected; however, both show limitations in achieving high conversions – even at very long polymerization times – plateauing at approximately 50% and 40%, respectively. On the other hand, addition of the initiator directly to the mold was shown to increase the conversion and reduce the polymerization time dramatically.

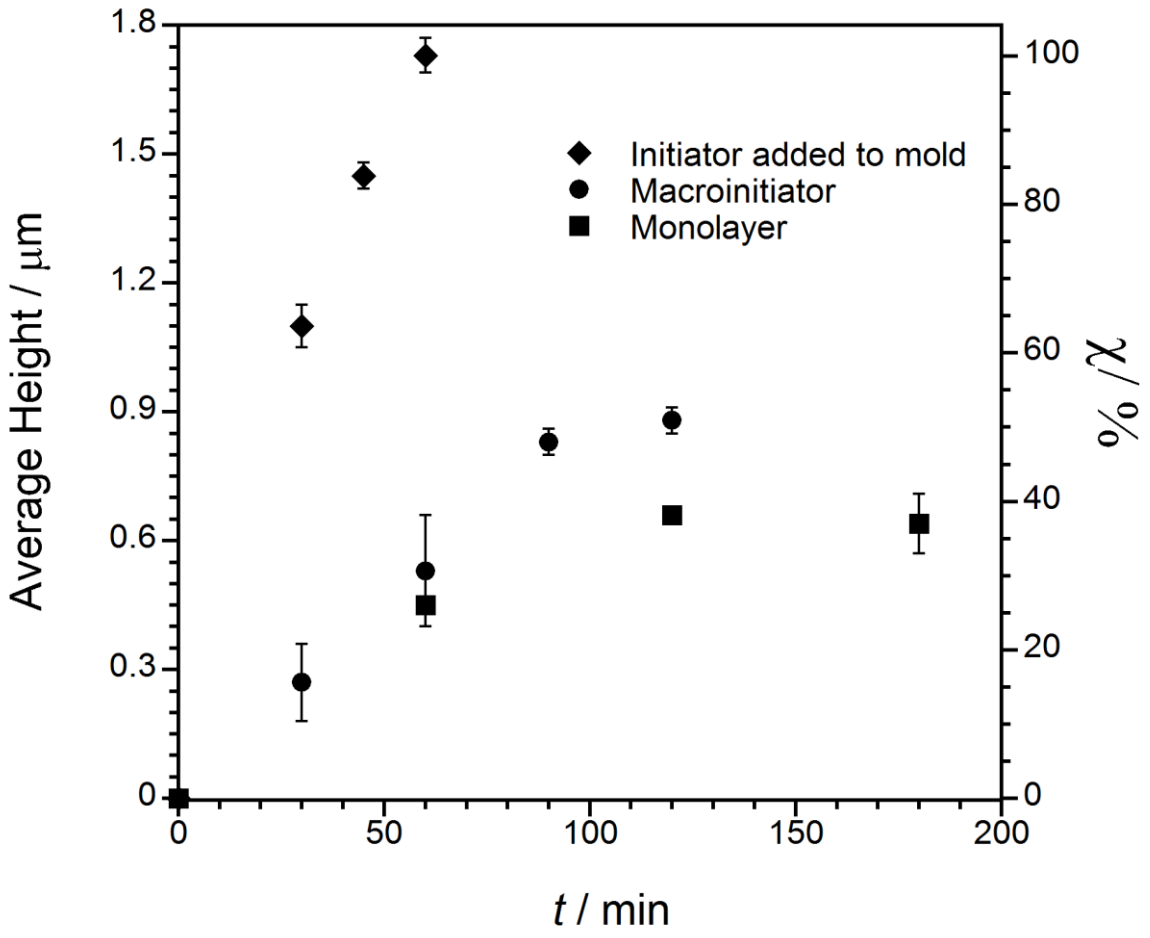

Figure 4 Effect of polymerization time on feature height for the three different initiation approaches, namely monolayer initiation, macroinitiation, and a combination of macroinitiation and addition of initiator to the mold. Polymerizations were performed at room temperature[15].

These substrates were characterized with SEM and AFM. Figure 5 below shows the original DFEA master (a) and the corresponding PNBF8 film (b). Expanded areas of b) are shown in c) and d) to demonstrate the uniformity of the surface. AFM comparisons of the feature heights for the film, mold, and master are shown in e), and an image of the PNBF8 film tilted at 45º to the surface normal is shown in f) to illustrate the film thickness.

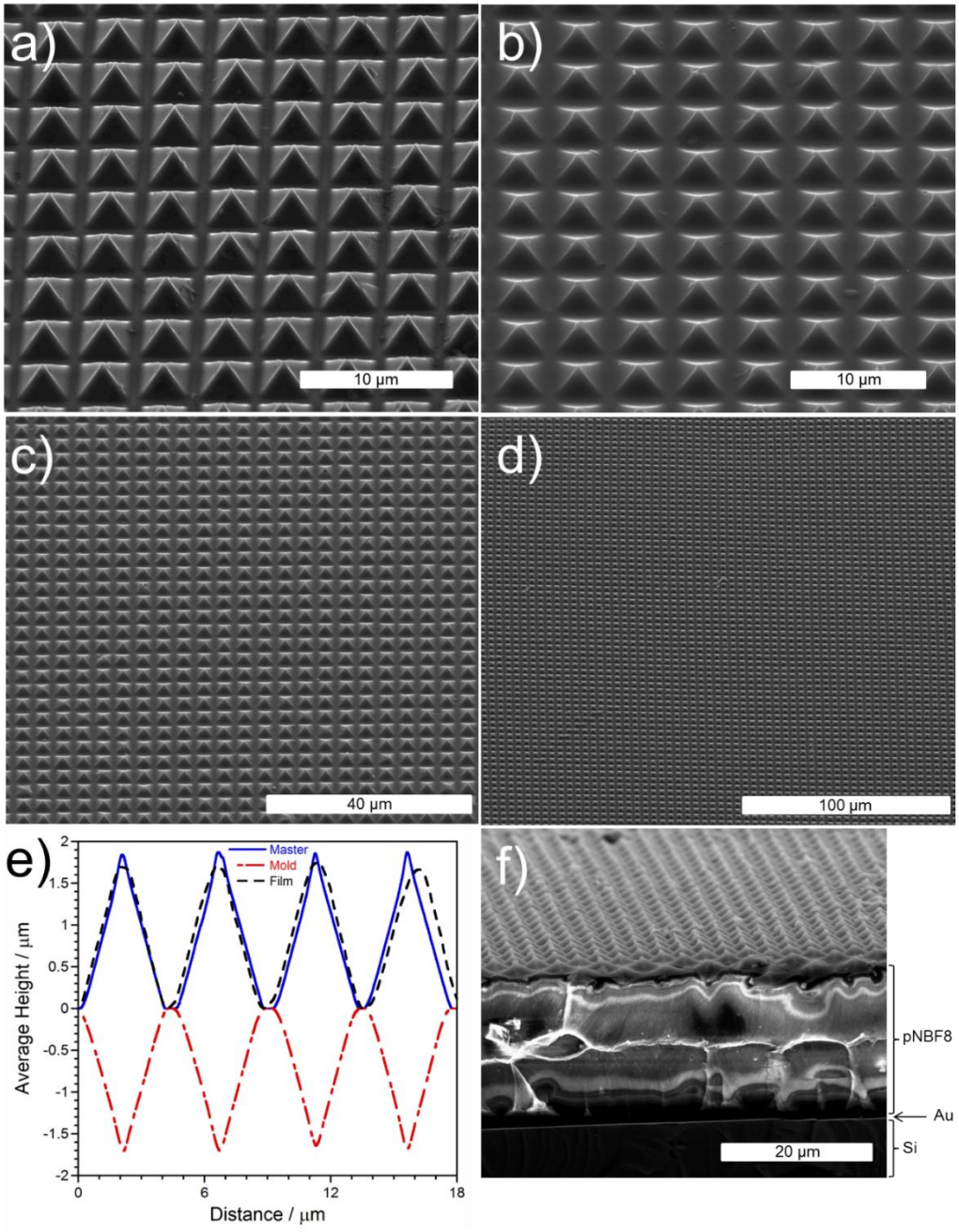

Figure 5 Scanning electron microscopy characterization of a) the surface morphology of DFEA master, b) resulting PNBF8 film reproducing the surface topography of the DFEA master shown in a). c) and d) scanning electron micrographs showing expanded areas from b). e) AFM line profiles of DFEA master in a), composite mold, and PNBF8 film in b), f) cross-sectional SEM image of the PNBF8 film in b). The SEM images in a), b), c), and d) were taken at a 45° angle with respect to surface parallel; f) was taken at 85°. All AFM measurements were performed in tapping mode. The error bars of the AFM line profiles are not shown for clarity of the plot. The error is within 3.5%[15].

As is shown by AFM that the average height of the pyramidal structures was greatest for pyramids grown with the combination of macroinitiation and an initiator-loaded mold (1.73 ± 0.04 μm), whereas those grown using only macroinitiation or monolayer initiation were limited to 0.88 ± 0.03 μm and 0.64 ± 0.07 μm, respectively. The plateau in conversion is reached at a polymerization time of 120 min and 90 min, contrarily, the macroinitiation/initiator-loaded mold approach reached almost complete conversion in 60 min. The difference in the kinetics of these reactions emerges because of the varied amount of initiator, which likewise shifts the ratio between chain growth and termination.

Elevated temperature was also investigated as a possibility for attaining higher conversions without the need for initiator loading of the mold. Films based on DFEA masters were grown using macroiniated μMSIP at 55 ºC rather than at room temperature. Their SEM and AFM characterization is shown in Figure 6 below. The film shows similar topography, dominated by pyramids at the outermost surface. However, the line profile in c) reveals that only incomplete conversion was realized, with the pyramids having ~ 60% of the volume from the composite mold. This incomplete conversion suggests again that the ratio of monomer to initiator is adequately high for termination reactions to overcome propagation. While elevated temperature did facilitate larger conversion and feature height than a macroinitiation approach carried out at room temperature, the success paled in comparison to the conversions shown for initiator loading of the mold.

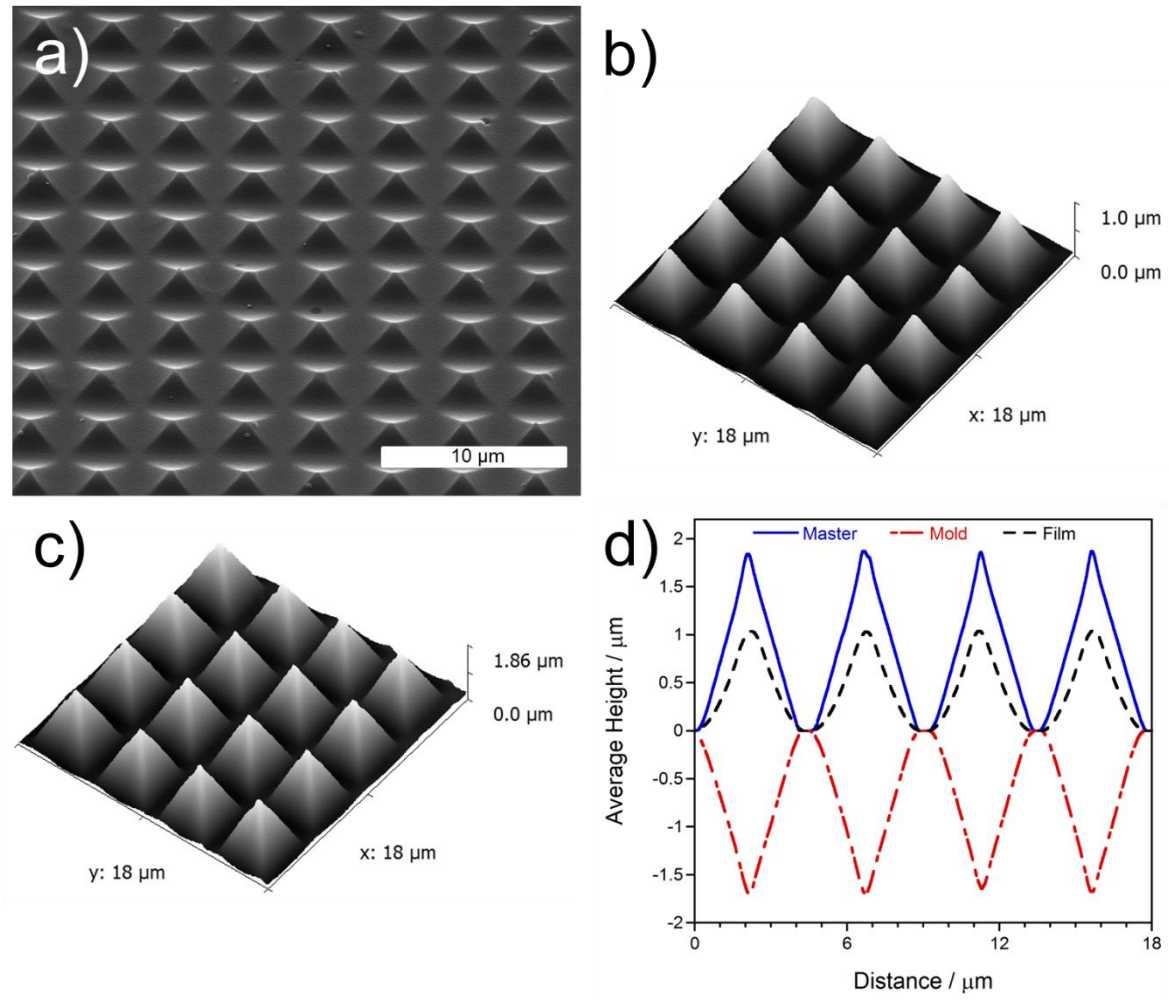

Figure 6 Surface topography of a textured film polymerized solely from a surface-bound macroinitiator at 55 °C for 1 h. a) Scanning electron microscopy image showing the surface morphology of the resulting film. b) 3D AFM image of the film in a), c) 3D AFM image of the DFEA master, d) AFM line profiles of DFEA master, composite mold, and PNBF8 film. The SEM images were taken at a 45° angle with respect to surface parallel. All AFM measurements were performed in tapping mode. The error bars of the AFM line profiles are not shown for clarity of the plot. The error is within 3.5%[15].

To validate this result, AFM line profiles were generated for PNBF8 films polymerized at 55º, 40º, and 21 ºC using both the monolayer-initiated and macroinitiated approaches. These are shown in Figure 7 below. In both cases, the height of the resulting pyramids increases as the temperature increases because the propagation reaction has a higher activation energy than the

termination reaction. Consequently, higher temperatures have been shown to accelerate the growth of PNBF8 films. For instance, increasing the polymerization temperature from 21 to 55 ºC increases the average height of the pyramids by a factor of ~2.17 for the monolayer-initiated approach and ~1.46 for the case of macroinitiation. This effect may also be associated with increased activity of the initiator at higher temperatures.

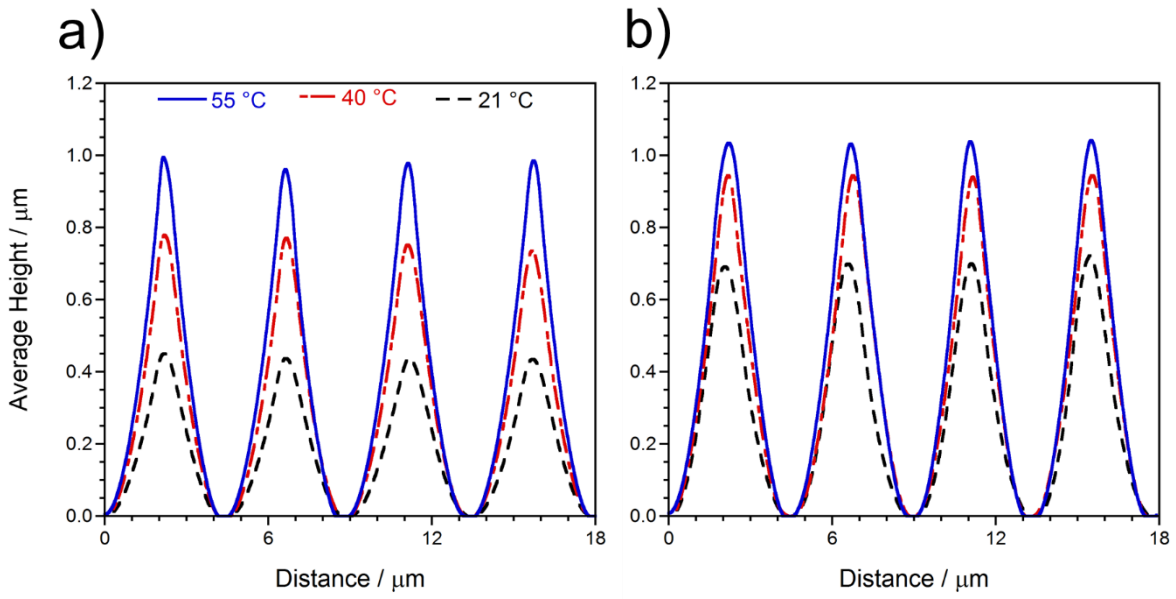

Figure 7 Temperature effects on the growth of pyramidally-textured PNBF8 films formed from a monolayer (a) or a macroinitiation (b) approach. Polymerizations were performed for 1 h in all cases. Error bars are not shown for clarity of the plot. The error is within 3.5%[15].

Additionally, the benefit of macroinitiation is attenuated at higher temperatures. At 21 ºC, the macroinitiation technique offers average pyramid heights 0.27 µm larger than those initiated from a monolayer, whereas at 55 ºC the macroinitiated film heights are only 0.07 µm larger. This trend indicates that the initiator species located nearest the interface react extremely rapidly as a consequence of the increased activity of the catalyst at higher temperatures. They likely form a

growing polymer that occludes the initiator species buried more deeply within the polymer film, mitigating some of the value of the added initiator species, and the macroinitiated films approach those of the monolayer films with increasing temperature.

Ultimately, purely surface-initiated cases of the polymerization are limited in their ability to achieve high conversions because chain termination reactions limit the propagation. This can easily be addressed by adding a tremendous excess of initiator to the mold, enabling one to reproduce feature heights that closely match that of the original master. For this work, 100% reproduction of the original feature height was desired in all cases, and the initiator loading of the mold approach was used exclusively (in combination with monolayer surface activation) to fabricate the PNBF8 films.

In addition to the DFEA substrates molded above, Klarite surfaces were also used as masters to demonstrate the effectiveness of this approach for reproducing the inverse architecture of the DFEA surface, that is, inverse pyramidal wells on the surface as opposed to the upright pyramids of the DFEA. Figure 9 below shows PNBF8 films based on Klarite masters grown using macroinitiation (55 ºC, 60 min). The films display similar inverted pyramids to the master, with the structures achieving approximately 63% of the corresponding height under these reaction conditions.

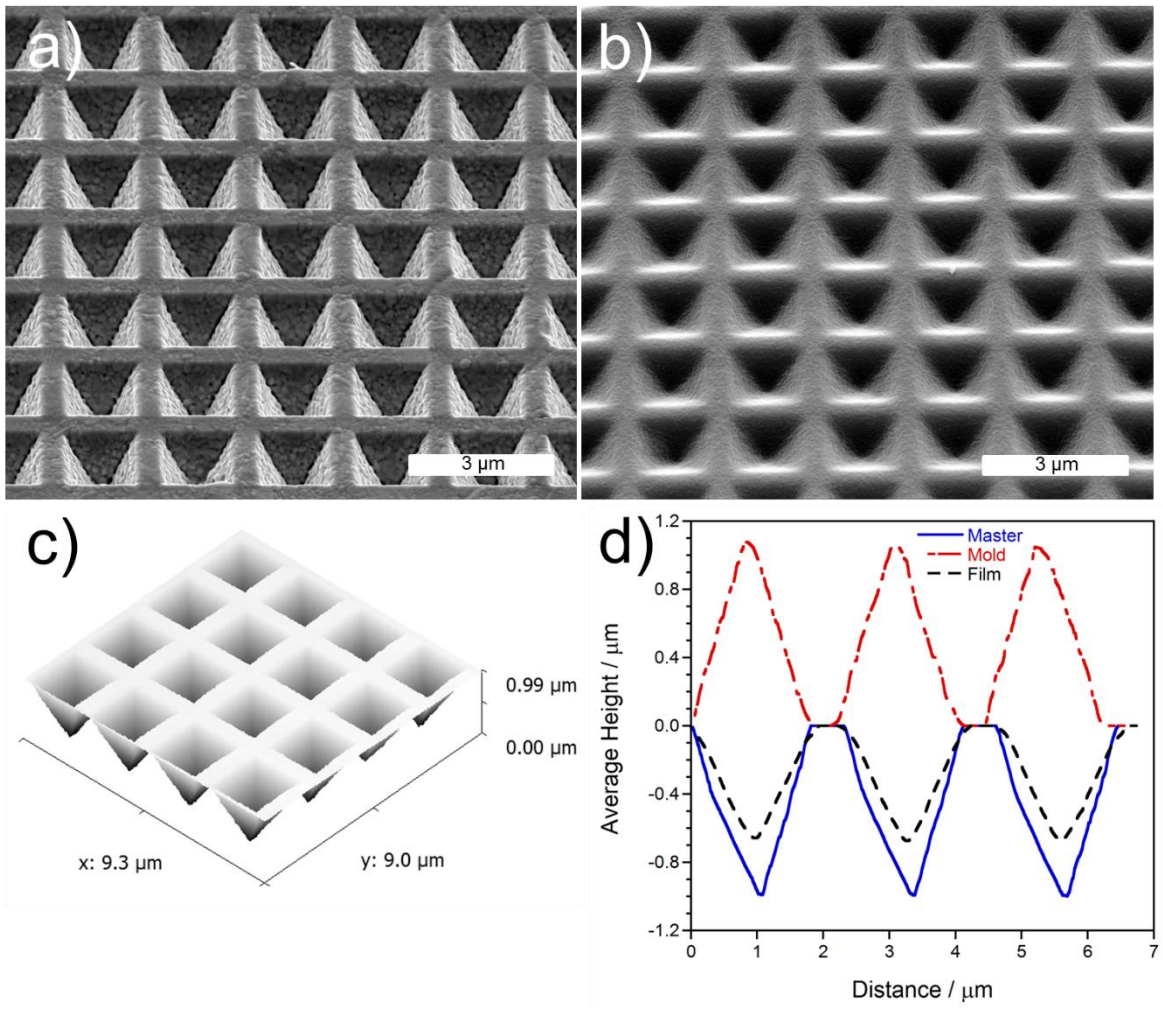

Figure 8 Surface topography of Klarite® and its corresponding µMSIP film. Scanning electron microscopy image of a) the surface morphology of Klarite® master, b) resulting polymer film, c) 3D AFM image of Klarite® master, d) AFM line profiles of Klarite® master d) AFM line profiles of Klarite® master, composite mold, and PNBF8 film. All AFM images were taken in tapping mode. The SEM images were taken at a 45° angle with respect to surface parallel. Error bars are not shown for clarity of the plot. The error is within 3.5%[15].

While the DFEA and Klarite substrates are useful because of their well-defined dimensions and geometry, they lack features necessary for exhibition of the unique surface properties associated with surface structuration – namely superantiwetting behavior. To demonstrate the applicability of µMSIP to surfaces bearing such architectures, two plant leaves –

those of *Trifolium repens* and *Aristolochia esperanzae* – were also reproduced with µMSIP.

Characterization of these surfaces is shown in Figures 10 and 11 below.

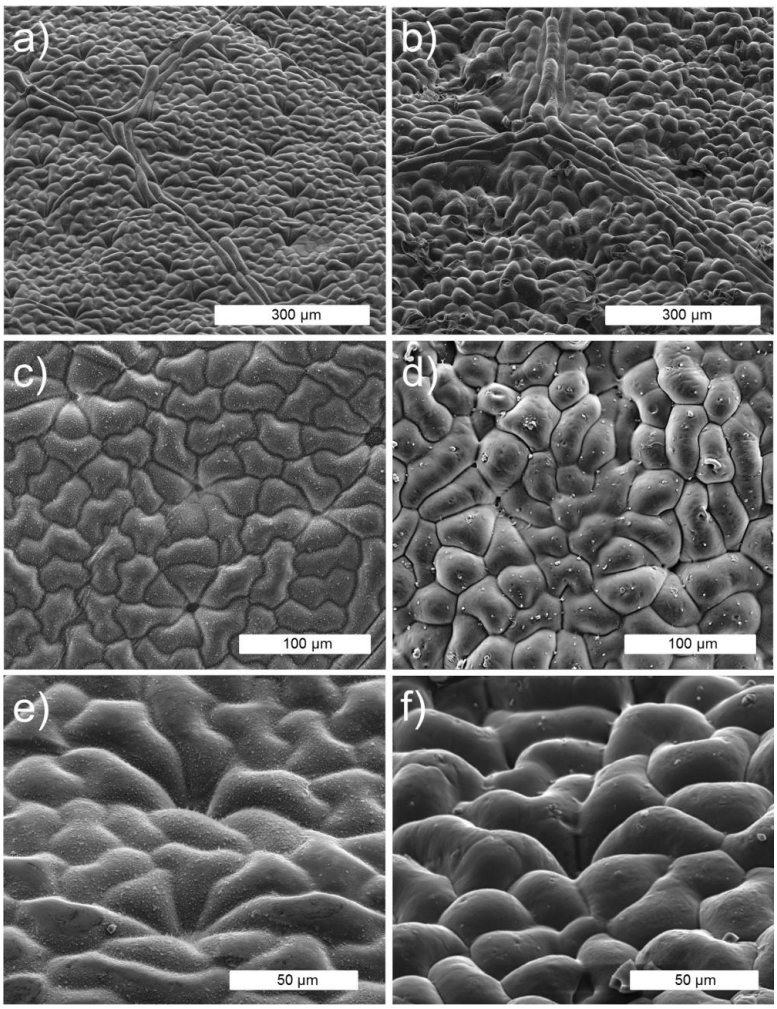

Figure 9 Scanning electron microscopy images showing the morphological characteristics of the adaxial surface of a,c,e) a fixed Aristolochia esperanzae leaf and b,d,f) its corresponding PNBF8-textured film. Tilted images (a,b,e,f) were taken at 45° with respect to the surface parallel[17].

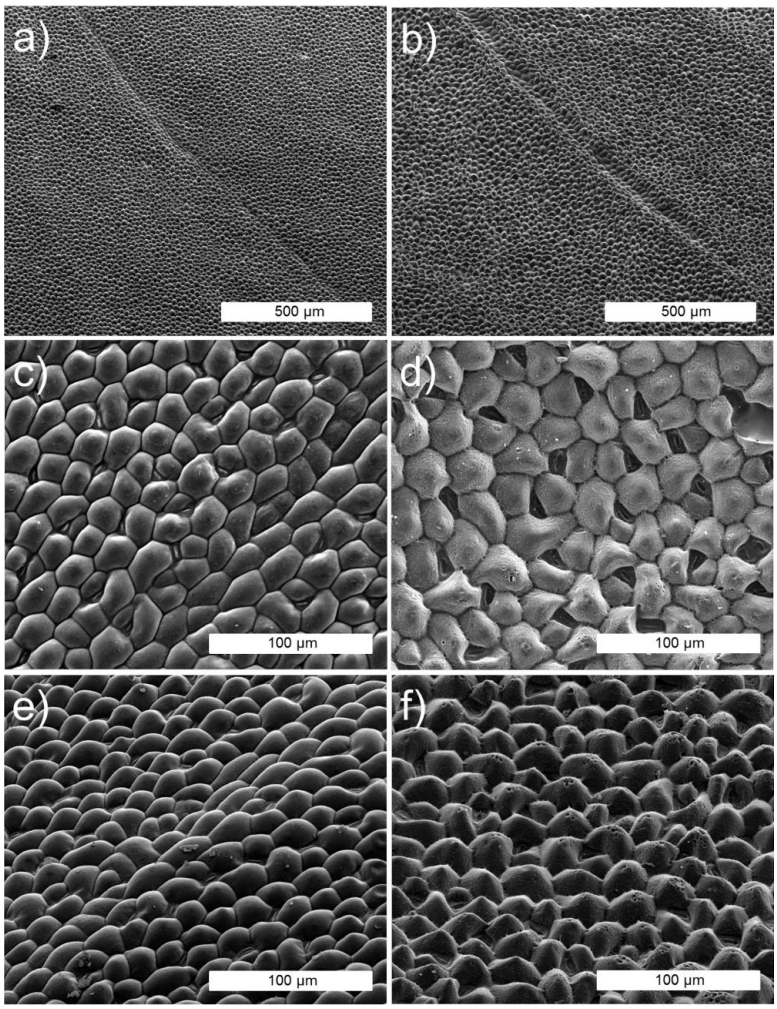

Figure 10 Scanning electron microscopy images showing the morphological characteristics of the adaxial surface of a,c,e) a fixed Trifolium repens leaf and b,d,f) its corresponding PNBF8-textured film. Tilted images (a,b,e,f) were taken at 45° with respect to the surface parallel. The polymer coating was not produced from the leaf shown in (a), (c), and (e)[17].

1.6.1 Surface Reactions of n-Alkyltrichlorosilanes

n-Alkyltrichlorosilanes have drawn significant research interest in recent decades, ode to their reactivity on a variety of surfaces. Monolayers of organosilanes have been formed on surfaces including: silicon oxide, aluminum oxide, quartz, glass, mica, zinc selenide, germanium oxide, and gold[18]. Additionally, monolayers with modified terminal groups are possible for SAMs of alkyltrichlorosilanes, enabling the engineer to control the surface chemistry exhibited by the monolayer. Terminal functional groups including halogens, cyanide, thiocyanide, methyl ether, acetate, thioacetate, α-haloacetate, vinyl, trimethylsilylethynyl, methyl ester, and *p*-chloromethylphenyl have been reported for alkyltrichlorosilane SAMs, and partially fluorinated alkyltrichlorosilanes have also used in monolayer formation[18]. Patterned SAMs have even been prepared by microcontact printing (μCP) on Al_2O_3/Al, SiO_2/Si, and TiO_2/Ti[18].

In spite of the abundance of research on these systems, substantial gaps in understanding remain. This is due in large part to reproducibility problems, which arise as a because of nuances in the mechanism and the need for precise control of reaction parameters including moisture content, solvent, and temperature. The mechanism is complicated by the coupling of polymerization with surface anchoring – not to mention the self-assembly and van der Waals interactions introduced by the alkyl chains – and the relations of these processes with one another is considered the primary source of reproducibility problems[18]. On top of that, self-assembly is not the only reaction these organosilane derivatives can undergo at the solid-liquid interface. Covalent attachment and vertical polymerizations are also possible[19]. Employing this vertical polymerization phenomenon to extremes never previously demonstrated is one of the primary techniques used to fabricate master surfaces for reproduction with μMSIP.

2 Materials & Methods

2.1 Experimental Procedures

2.1.1 Micromolding Surface-Initiated Polymerization

2.1.1.1 Phase I: Micromolding

The micromolding step is performed using hard polydimethylsiloxane (hPDMS). The molding process proceeds as follows. First, 3.4 g of [(7–8% vinylmethylsiloxane)-(dimethylsiloxane)] copolymer, two drops of 1, 3, 5, 7-tetramethylcyclotetrasiloxane, and 1 drop of platinum divinyltetramethyldisiloxane were mixed vigorously for at least 8 minutes in a small plastic beaker. As the components are mixed, significant quantities of air become entrapped in the solution. The bubbles are removed by placing the mixing beaker in a desiccator connected to a vacuum line and then evacuating the system. As air is removed, substantial bubbling occurs at the solution surface, and evacuation continues until bubbles are no longer visible. Because the reduction of pressure causes bubbles to rise and expand, the vacuum was broken and restored several times to prevent spillover.

After the first degassing step, 1 g of [(25–30% methylhydrosiloxane)-(dimethylsiloxane)] was added to the mixture, and a glass rod was again used to stir the pre-polymer for 3 minutes. Typically, the solutions were degassed again prior to pouring over the master substrates, following the same procedure as above. After this, the pre-polymer was poured over the master surface, and hPDMS covered substrate was again placed in the desiccator and evacuated until no bubbles could be observed. Curing of the hPDMS was accomplished by placing the hPDMS covered substrate into an oven at 60^{o} C for 10 minutes.

In previous work, an additional step was employed wherein a layer of Sylgard 184 PDMS was added on top of the cured hPDMS to form a thicker polymer composite. However, it was found that no substantial difference could be observed between those hPDMS molds having this super-layer and those that did not. Therefore, this step has been omitted from the process because it adds a substantial amount of time (> 6 h) to the molding process.

2.1.1.2 Phase II: Surface Initiated Polymerization

To prepare the gold substrates, silicon wafers were washed with ethanol and water and then dried with a stream of nitrogen. The cleaned wafers were loaded into a CVC-PSM66 evaporator. Chromium and gold were evaporated onto the wafer sequentially with thicknesses of 100 Å and 1250 Å, respectively. An evaporation rate of 1 – 2 Å/s was used, with a base pressure less than 4×10^{-6} torr. Samples of the gold-coated silicon wafers were cut to approximately 1.2 cm × 3.5 cm for use.

An initiator-activated self-assembled monolayer (SAM) was then fabricated on the gold surface to induce polymerization. Gold-coated silicon samples were immersed in 1 mM 4-mercapto-1-butanol in ethanol for at least 1 hour to form a hydroxyl-terminated SAM on the gold surface. Upon removal, the samples were rinsed with ethanol and dried in a stream of nitrogen. Next, the hydroxyl-coated surface was exposed to a 5 mM solution of NBDAC in DCM for at least 30 minutes, resulting in ester linkages of the norbornenyl groups to the underlying hydroxyl monolayer. These samples were rinsed with DCM and ethanol before drying in a stream of nitrogen. To render the surface active for SI-ROMP, initiator was immobilized on the surface by exposure to a 5 mM solution of Grubbs 2nd generation catalyst in DCM for 10 min. As the samples were immersed in the Grubbs catalyst solution, a dilute solution of Grubbs Catalyst in DCM was added to the mold and the solvent was allowed to evaporate. This allows initiator to be

deposited in the recesses of the mold and results in improved feature-height and reproduction fidelity of the final polymer film. Just as the activation step approaches completion, sufficient quantities of NBF8 monomer were added to the mold. After activation (and less than 30 seconds after NBF8 addition), the samples were quickly rinsed with DCM, dried with nitrogen, and pressed against the monomer-filled mold. Polymerization was allowed to proceed to completion (~2 h) before the mold was removed. Samples were then rinsed with DCM, ethanol, and water and then dried with nitrogen prior to storage. The polymerization process was carried out under ambient conditions.

2.2 Characterization

2.2.1 Wetting Measurements

Contact angle measurements were performed with a Rame-Hart contact angle goniometer using deionized water and hexadecane as probe fluids.

2.2.2 Scanning Electron Microscopy

SEM images were collected using a Hitachi S4200 scanning electron microscope. Substrates were coated with gold prior to imaging.

2.2.3 Fourier Transform Infrared Spectroscopy

Attenuated total reflectance Fourier transform infrared spectroscopy (ATR-FTIR) spectra were collected using a Nicolet IR200 FTIR with a germanium crystal.

2.3 Materials

4-Mercapto-1-butanol (97%), Grubbs catalyst 2nd generation (1,3-Bis-(2,4,6-trimethylphenyl)-2-(imidazolidinylidene) (dichlorophenylmethylene) (tricyclohexylphosphine) ruthenium), trans-3,6-endomethylene-1,2,3,6-tetrahydrophthaloyl chloride (NBDAC, 97%),1H,1H,2H-perfluoro-1-decene (99%), and hydroquinone were used as received from Sigma-Aldrich. Tridecafluoro-1, 1, 2, 2-tetrahydrooctyl-1-trichlorosilane (TFOCS) was purchased from UCT Specialties. Gold shot (99.99%) was obtained from J&J Materials, and silicon (100) wafers were purchased from WRS Materials. Deionized water (16.7 MΩ) was purified with a Modu-Pure filtration (Continental Water Systems Corporation) system and used for rinsing. Ethanol (200 proof) was obtained from AAPER and used as received. Nitrogen gas was obtained from AL compressed gases. The synthesis of 5-(perfluorooctyl)norbornene (NBF8) was performed as described above. [(7–8% vinylmethylsiloxane)-(dimethylsiloxane)] copolymer, 1, 3, 5, 7-tetramethylcyclotetrasiloxane, platinum divinyltetramethyldisiloxane, and [(25–35% methylhydrosiloxane)-(dimethylsiloxane)] were purchased from Gelest, Inc. Dow Corning Sylgard® 184 Silicon Elastomer Kit was obtained from Ellsworth Adhesives.

3 Results & Discussion

3.1 Research Objectives

Fundamentally, the intentions of this research are broad. The crux is simply extending and optimizing a technique in its infancy – micromolding surface-initiated polymerization. Consequently, the success or failure of the work may seem ambiguous lacking an enumeration of more specific aims.

First, the value of techniques such as $\mu MSIP$ lies in their versatility. To date, this approach has only been used to reproduce four different surface architectures. These include:

1. Diamond field emitter arrays (pyramids)
2. Klarite (inverted pyramids)
3. *Aristolochia esperanzae*
4. *Trifolium repens*

The first two have well-defined architectures, offering the ability to characterize molding fidelity, and the latter two are surfaces taken from nature, allowing examination of water-repellency type properties. While these four surfaces were very useful for preliminary analysis, they lack many properties of interest to surface scientists, and further demonstrations of the technique's utility must be demonstrated. Additionally, each of these surfaces were "found" and replicated, rather than fabricated with their replication specifically in mind. This limits one to predetermined morphologies, rather than allowing the engineer to generate surfaces that may be tailored to their end goals. Consequently, one of the first and most basic of the objectives in this work was to fabricate novel surface architectures that could be used as masters for this replication process. Additionally, surfaces falling outside the umbrella of previous work (i.e. not micromachined or taken from nature) were also desired. Demonstrating successful reproduction

of either inorganic or metal-based surfaces would represent an extension of the technique to new territory.

Additionally, a major question remaining is whether μMSIP can be used to reproduce surfaces having re-entrant geometry. As explained, re-entrant geometry is an indispensable requirement for superantiwetting. In addition to re-entrance, the presence of both micro- and nanoscale roughness is also essential, and this also must be demonstrated by μMSIP. While superhydrophobicity was shown on one of the surfaces from previous work (*Aristolochia esperanzae*), substantial room for improvement exists in the realm of wetting properties. In this vein, my goals included achieving higher water contact angles than those from earlier work, as well as possibly achieving superoleophobicity. Neither would be attainable without truly re-entrant surfaces having both scales of hierarchical roughness, and developing such architectures was a critical aspect of this research.

3.2 Substrate Fabrication

Beginning to select candidate surfaces for molding represented a major challenge initially. This process necessarily began with a bit of educated guesswork, and to facilitate the selection process, a number of desired features were outlined. With those in mind, we were able to narrow down the possibilities and start experimenting with the most promising options. Some such characteristics include:

1. Never previously reproduced using $\mu MSIP$
2. Uses readily available materials
3. Requires no advanced machinery, only basic lab ware
4. Quick, facile, repeatable procedure

5. Tunability of surface morphology
6. Potential for superhydrophobic/superoleophobic surfaces
7. Not biological in nature

Initially, focus was on electrochemical possibilities, however, this shifted over time due to obstacles with repeatability. As work proceeded, several other intriguing options presented themselves and offered better results. It was noticed that n-octadecyltrichlorosilane used to modify several of the electrochemically generated surfaces was polymerizing during the molding process. While this was found to obfuscate the surface of interest, it led to a compelling architecture of its own. These regions were ultimately found to give the largest contact angles achieved, so vertical polymerization of n-octadecyltrichlorosilanes became one of the predominant approaches used for fabricating master surfaces for molding.

3.3 Aqueous Ammonia Etching of Copper Foils

Copper foil was selected as a potential inorganic substrate for surface modification because of its availability and low cost. Aqueous ammonia etching was investigated due to its demonstrated success in forming a surface which displayed underwater superoleophobicity[20]. Copper foils were therefore immersed in aqueous ammonia for various times to assess the results. In all cases, the process began with an initial dissolution of copper ions causing the solutions to develop a deep blue color, characteristic of aqueous copper. The anticipated mechanism – oxygen adsorption corrosion of copper – involved the following steps[20]:

$$Cu + \frac{1}{2}O_2 \rightarrow [Cu - O]$$

$$[Cu - O] + 4\,NH_3(aq) + H_2O \rightarrow Cu(NH_3)_4^{2+} + 2\,OH^-$$

$$Cu(NH_3)_4^{2+} + 2\,OH^- \rightarrow CuO \downarrow + 4\,NH_3 \uparrow + H_2O$$

While the results of previous work were indeed corroborated – after ~ 24 h, black CuO films were observed – an interesting phenomenon was discovered if the reaction was allowed to proceed for longer times. As the aqueous ammonia solution gradually evaporated, the black oxide surface was replaced with a bright blue patina. Examples of these systems during the etching process are shown in Figure 11a below, and the surfaces resulting after various lengths of time are shown in Figure 11b.

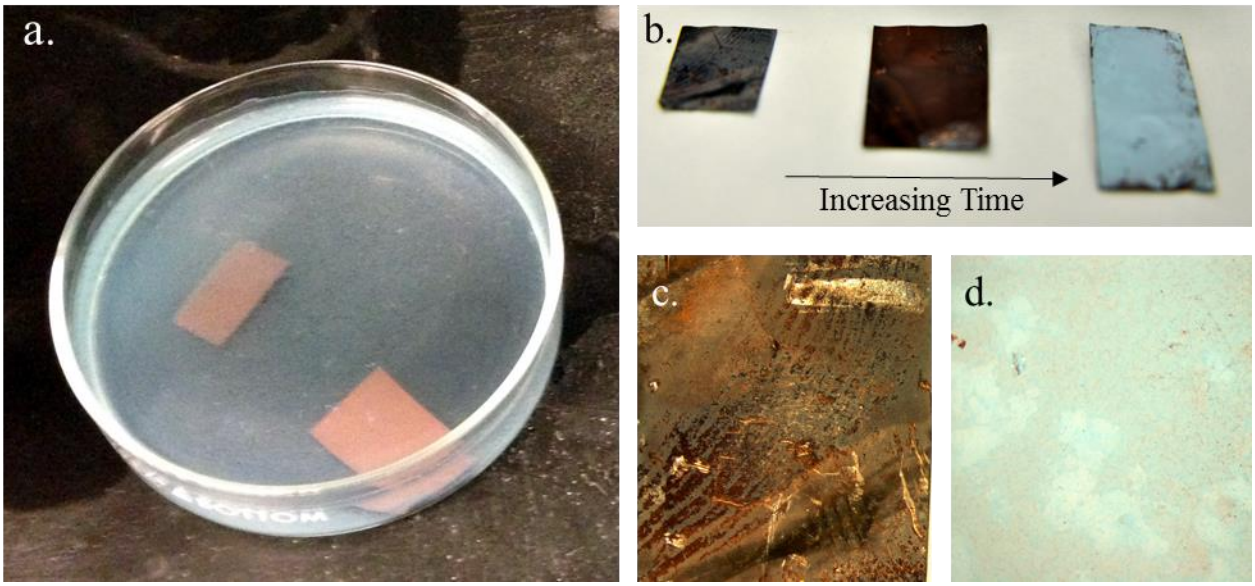

Figure 11 a) Aqueous ammonia etching of copper foils was carried out in a fume hood, open to atmospheric oxygen and evaporation b) as time elapses the surface of the foil develops from a black copper oxide surface (c) and a blue copper hydroxide patina (d) formed after evaporation

When analyzed using ATR-FTIR, it was found that the blue patina surfaces showed a tremendously large hydroxyl peak (3100-3400 cm^{-1}) that was not present for the blackened

samples, suggesting a surface comprised of copper hydroxide $Cu(OH)_2$ rather than CuO. This peak may be seen in Figure 12 below.

High contact angles could not be expected from such high-energy inorganic surfaces; however, it was expected that coating these with a material bearing aliphatic chains, such as an alkyltrichlorosilane or alkanethiol, might result in significant antiwetting properties. For this, n-octadecanethiol was initially chosen, and FTIR spectra of the surfaces were collected before and after treatment to verify the attachment of the aliphatic chains. Spectra taken after the treatment may be seen in Figure 12. For both the CuO and patina surfaces, peaks correlated to the C-H stretch may be found at 2919 cm^{-1} and 2850 cm^{-1}, indicating the adsorption of the alkanethiol was successful. These peaks were absent in the spectra taken prior to the treatment.

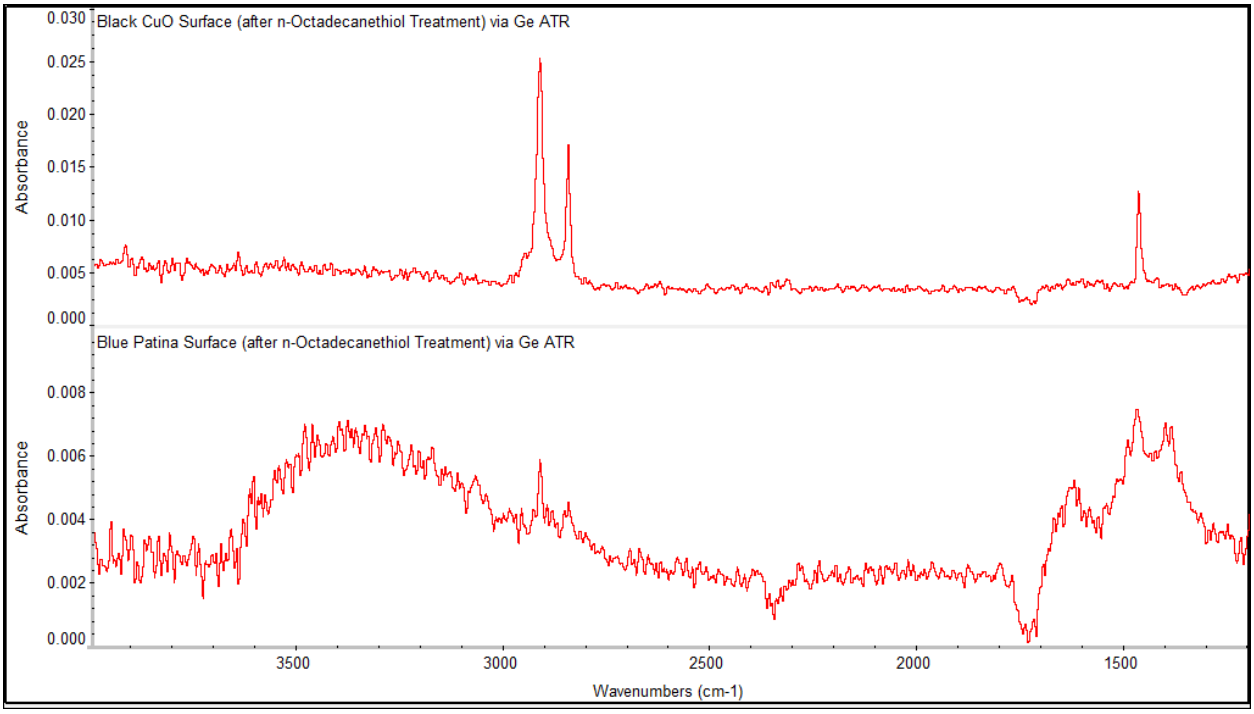

Figure 12 FTIR spectra for the black CuO surface (top) and blue patina surface (bottom) indicate successful adsorption of n-octadecanethiol

After the surface was made hydrophobic, the roughness enabled an increase in the contact angle and pronounced water repellency was observed. This may be seen from the water droplets at equilibrium in Figure 13 below. For the black CuO surfaces, advancing contact angles of 150º ± 4º were observed, and for the blue patina, an even higher contact angle of 162º ± 3º was found. These surfaces were highly hysteretic however, with receding contact angles on the order of 70º. The high hysteresis suggests poor or incomplete adsorption of the alkanethiol, resulting in regions of high surface energy scattered throughout the surface. These regions could result in pinning of the contact line, causing an apparent increase in the advancing contact angle while at the same time, dramatically reducing the receding contact angle. This could likely be solved, perhaps by treatment with an alkyltrichlorosilane or a fluorinated alkyltrichlorosilane instead, but fortunately, it represented only a trivial obstacle for this work. Through μMSIP, the surface architecture of these substrates would be ultimately reproduced with a final, uniform composition of PNBF8. It is clear from the advancing contact angles achieved that the surface architecture contributes to a dramatically elevated contact angle, and with the fluoropolymer composition, hysteresis due to isolated regions of high surface energy should be eliminated.

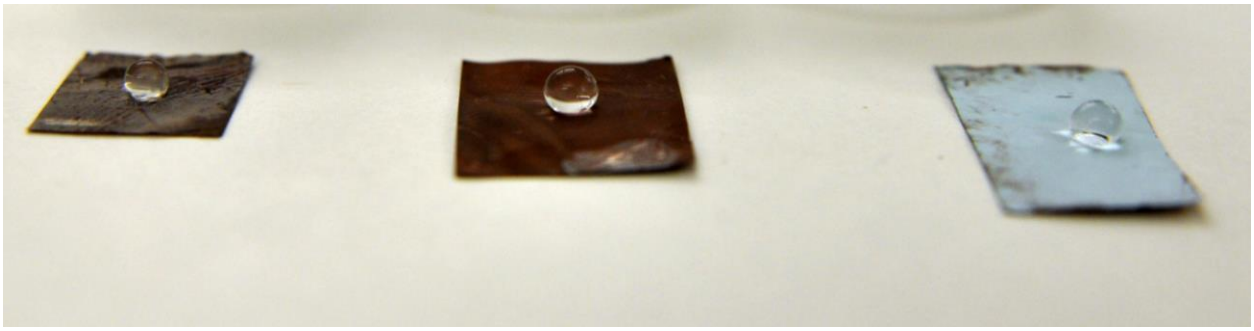

Figure 13 Water droplets at equilibrium on the ammonia-etched copper foils demonstrate the water-repellency of the surfaces after treatment with n-octadecanethiol

Scanning electron microscopy was performed to analyze the surface architecture of the unmodified copper foil, the blue patina surfaces, and the black CuO surfaces. In Figure 14 below, micrographs for the unmodified copper foils (left) and the blue patina (right) are shown at the same scale for comparison.

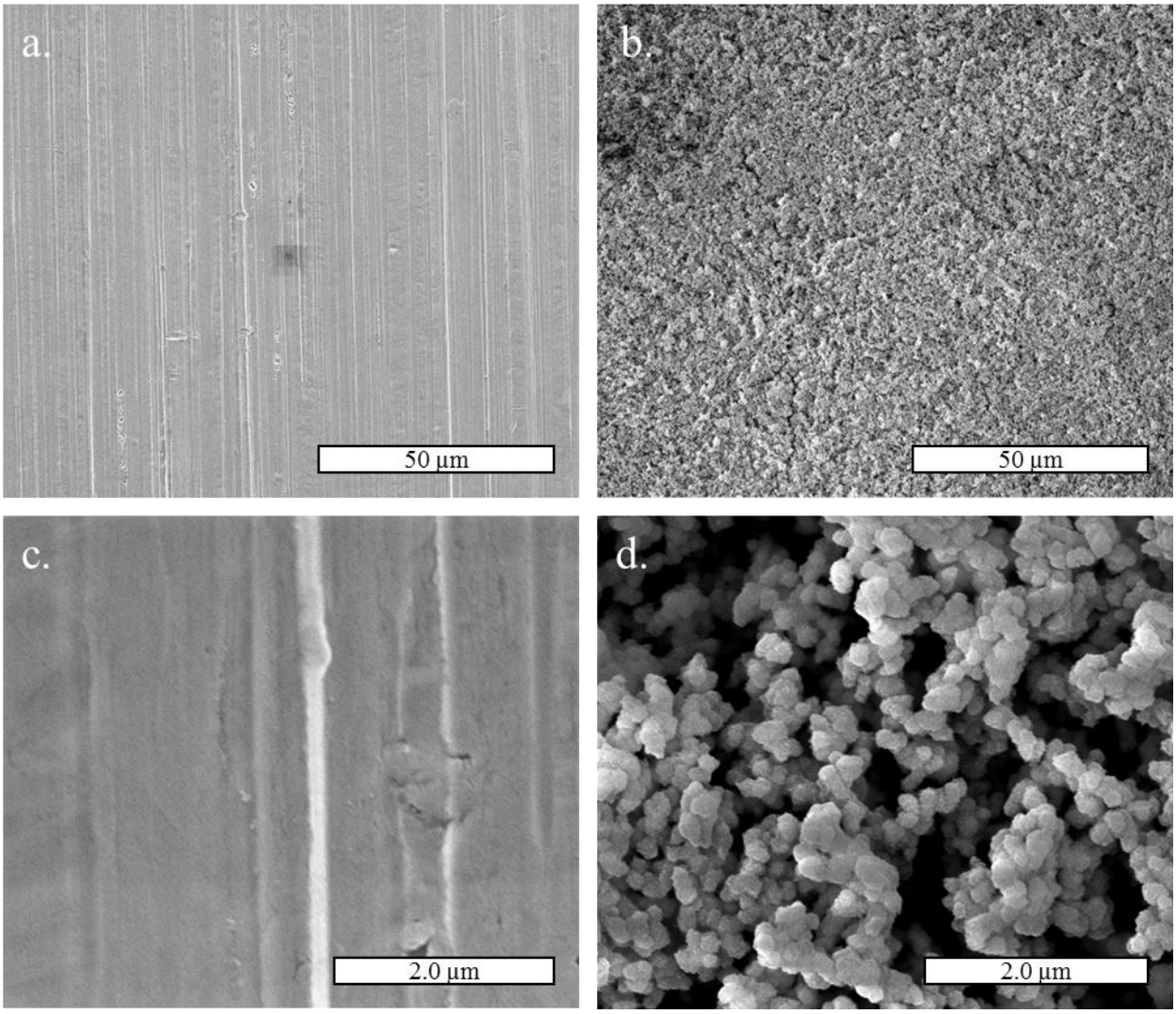

Figure 14 Scanning electron microscopy of plain copper foil (left) and blue patina surface resulting from aqueous ammonia etching (right).

Clearly, the plain foil surface shows little structuration beyond lines from rolling during manufacture. The patina surfaces however show substantial surface roughness emerging from a network of aggregated copper hydroxide nanoparticles approximately 300 nm in size. These nanoscale features may be seen in Figure 15 below, and, importantly, the blue patina surface clearly displays hierarchical roughness at both the micro- and nanoscales. This level of roughness is critical for superantiwetting, and was a key requirement for the surfaces to be used in μMSIP.

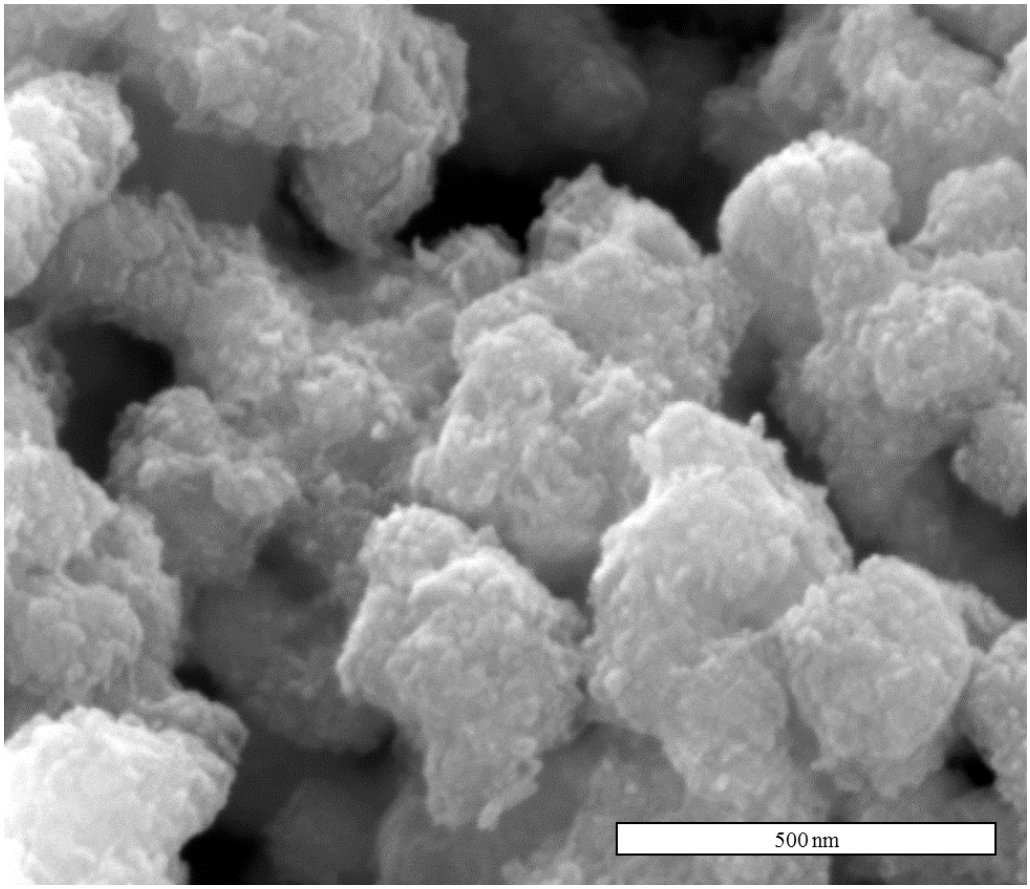

Figure 15 Scanning electron microscopy of the blue patina formed after aqueous ammonia etching of copper foils shows hierarchical roughness and a surface comprised of ~300 nm copper (I) hydroxide nanoparticles

SEM images of the black CuO foils show a markedly different surface architecture, as shown in Figure 16. These surfaces display what can best be characterized as nanohairs less than 100 nm in length and with diameters no larger than about 10 nm. Additionally, grain boundaries may be seen, with grain sizes on the order of tens of microns.

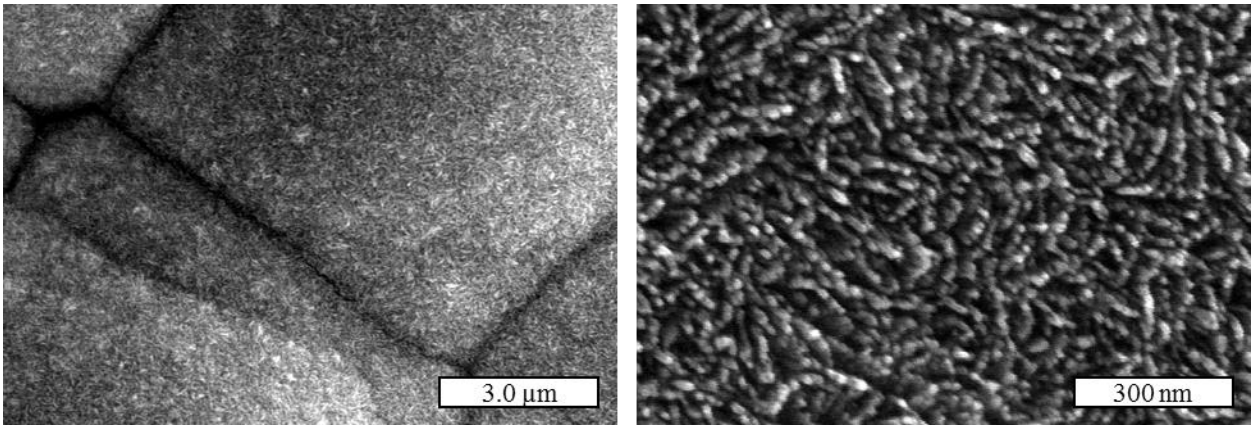

Figure 16 Scanning electron microscopy of black CuO foil surfaces show grains tens of microns in size coated with nanohairs ~ 100 nm long and ~10 nm in diameter

The micrographs of the black CuO surfaces explain well why the contact angle is substantially higher for the patina surfaces. While the nanoscale roughness is clearly present for the black CuO, the microscale roughness is substantially less pronounced. Additionally, the much thicker patina coating offers significantly improved re-entrance and much greater potential for trapped air pockets, which play an important role in superantiwetting. Clearly, the blue patina surfaces were better candidates for reproduction with µMSIP, having all of the properties established as desirable for this work.

3.4 PNBF8 Films Based on Etched Copper Foils

PNBF8 films were fabricated using molds of the blue patina surface formed by the aqueous ammonia etching procedure described above. However, the molding procedure employing hard PDMS had not yet been implemented, and the micromolding step was instead carried out with Sylgard 184 for these surfaces. This soft microfabrication process proved problematic, because the central reason that hPDMS became the primary material used for micromolding was that it offered better fidelity in replicating very small features – particularly those in the nanoscale. Some success was still achieved however, as can be seen in Figure 17 below. An image of the blue patina surface is shown at the right, and an image of a PNBF8 film based on such a surface is shown at the left.

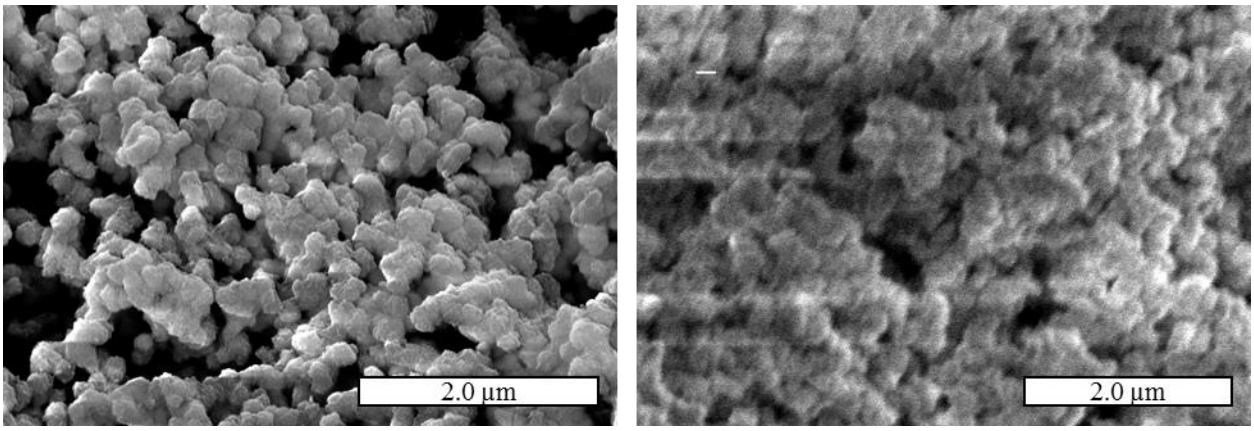

Figure 17 SEM images of a master blue patina surface (left) and a PNBF8 film reproduction of such a blue patina surface (right).

The general structure at the micron scale was reproduced with a fair degree of success, but the deeper crevices of the surface and many of the nanoscale features were lost. Further, the majority of the surface showed poorer reproduction than seen above, with only the outermost

asperities captured by the molding as well as with deep holes scattered across the PNBF8 film. Despite these major imperfections, traces of the original surface are still recognizable, and these results are still presented for a number of valuable insights they provide.

First, it seems apparent that the failure of these films came during the micromolding step of the process, because the images show that some regions of the surface architecture were captured successfully by the PNBF8, even some of the smaller features in the nanoscale. The SIP steps for both these films and the ODTS based films were carried out identically, suggesting that if the micromolding step had yielded an accurate negative reproduction, the PNBF8 would have been able to reproduce them. It is much more likely that the micromolding produced only a poor replica, and this is easily explainable given the fact that hPDMS was not used for these substrates. It is reasonable that if these foils were molded using the hPDMS procedure described above, the architectures would have been reproduced more faithfully. Unfortunately, work with these copper-based surfaces was halted in favor of other candidate substrates, particularly those based on polymerized octadecyltrichlorosilane, because of difficulties with repeatability of producing the blue patina surfaces and the long time required to make them.

Still, these results do suggest that in principle, inorganic or metal-based substrates could be successfully reproduced with the hPDMS molding procedure described above. This shows the value of the hPDMS approach if one is attempting to mold very small features, despite its relatively more complicated preparation. The potential surfaces that could be generated using metals and other inorganic materials are innumerable, and the demonstration of the applicability of μMSIP to such substrates offers a useful starting place for future research.

3.5 Vertical Polymerization of n-Octadecyltrichlorosilane

n-Octadecyltrichlorosilane (ODTS) is a staple in any surface modification laboratory due to its well-established ability to form monolayers on a variety of substrates, including silica and many inorganic oxides and hydroxides. ODTS is typically employed for modifying high-energy surfaces, upon which it forms a monolayer with its terminal methyl group exposed. This leads to a low-energy surface with many practical applications.

In trying several approaches for rendering a copper (II) hydroxide substrate hydrophobic, one procedure involved application of a drop of pure n-octadecyltrichlorosilane (ODTS) directly onto the inorganic surface prior to micromolding. An example of one such mold is shown in Figure 18a below. While the intended substrate was not molded successfully, it was noticed that the region surrounding the copper foil showed discoloration. Magnification of the mold (shown in Figure 18.b) revealed that this region showed a negative image of some supramolecular structure, distinct from the comparatively smooth surfaces of the polypropylene dish or the scotch tape used to mount the sample. When the fluoropolymer reproduction was completed, scanning electron microscopy showed the elaborate network depicted in Figures 18c and d. The structuration, characterized as a network of interpenetrating fibrils.

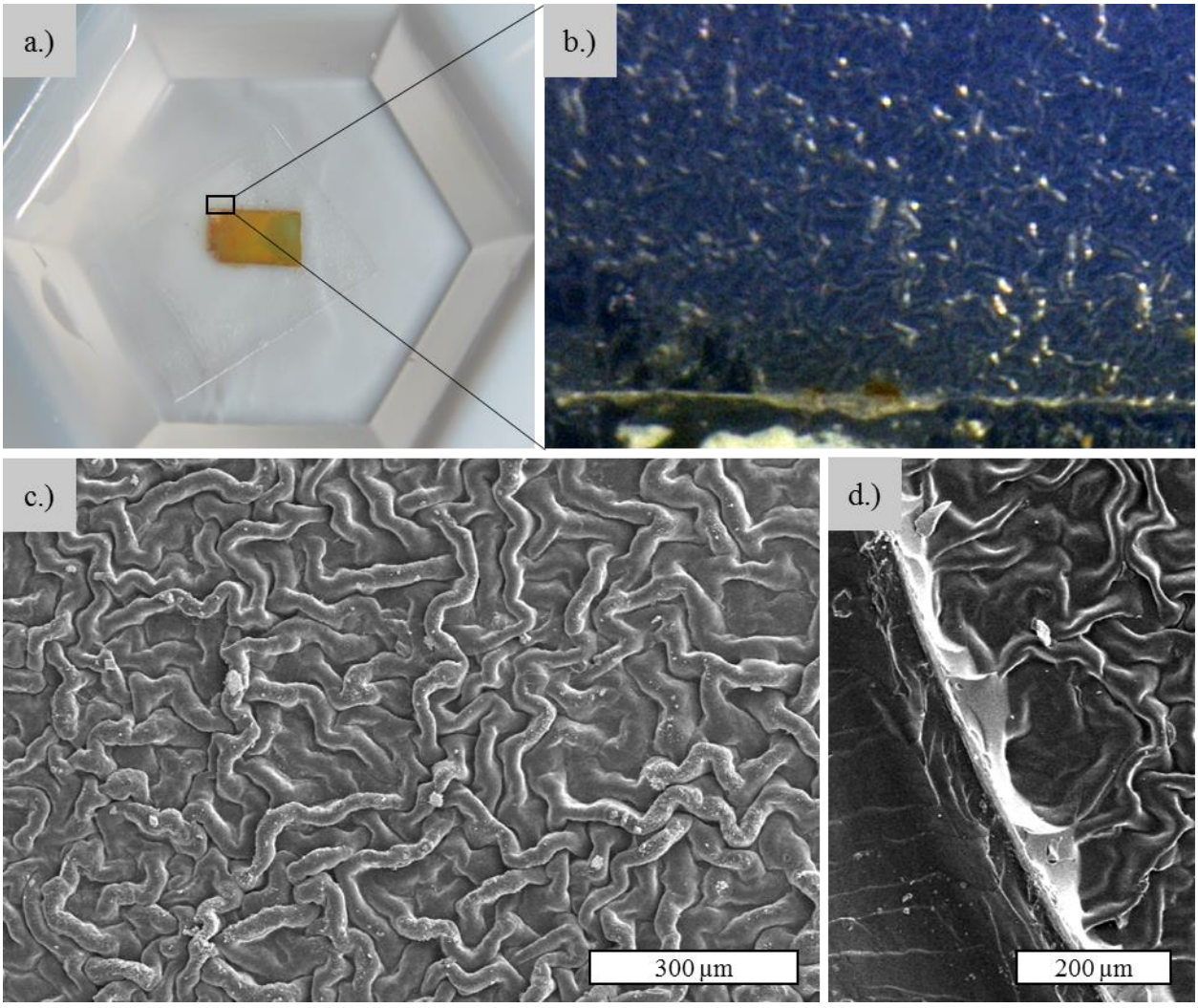

Figure 18 a) Copper foil sample for uM, modified with a drop of pure ODTS b) enlargement of the region surrounding the foil sample shows a negative image of some supramolecular structure, attributed to ODTS polymerization c) PNBF8 reproduction of the image shown in b). d) SEM image of the PNBF8 film showing the edge seen in the lower portion of b)

The structures above were superhydrophobic, possessed apparent re-entrance, differed substantially from and had smaller features than previous surfaces reproduced by µMSIP. The architecture self-assembled under ambient conditions; it reacts quickly; and its familiarity, cost, and accessibility all made it an ideal candidate for substrate fabrication such that further investigation was warranted.

Several major questions existed as a starting place for controlling the assembly of these structures and subsequently utilizing them for surface reproduction. While the underlying mechanism is reasonably well understood and poly(n-alkyl)siloxanes have been characterized to a certain extent, they have never been observed to form these structures. The first step to understanding this process was to develop a protocol that could reliably produce structures that would be useful for μMSIP. The initial result was discovered on the surface of scotch tape – poly(2-octylacrylate) – and it was important to demonstrate that this approach could be used to form films on more common laboratory substrates. Glass microscope slides were chosen for the known affinity for self-assembly of trichlorosilanes on these surfaces, and polypropylene was chosen to assess whether this procedure was viable even in the absence of surface hydroxyl groups. Film production was successful in both cases, and the general features of each appeared similar, independent of the substrate. These films are shown in Figure 19 below.

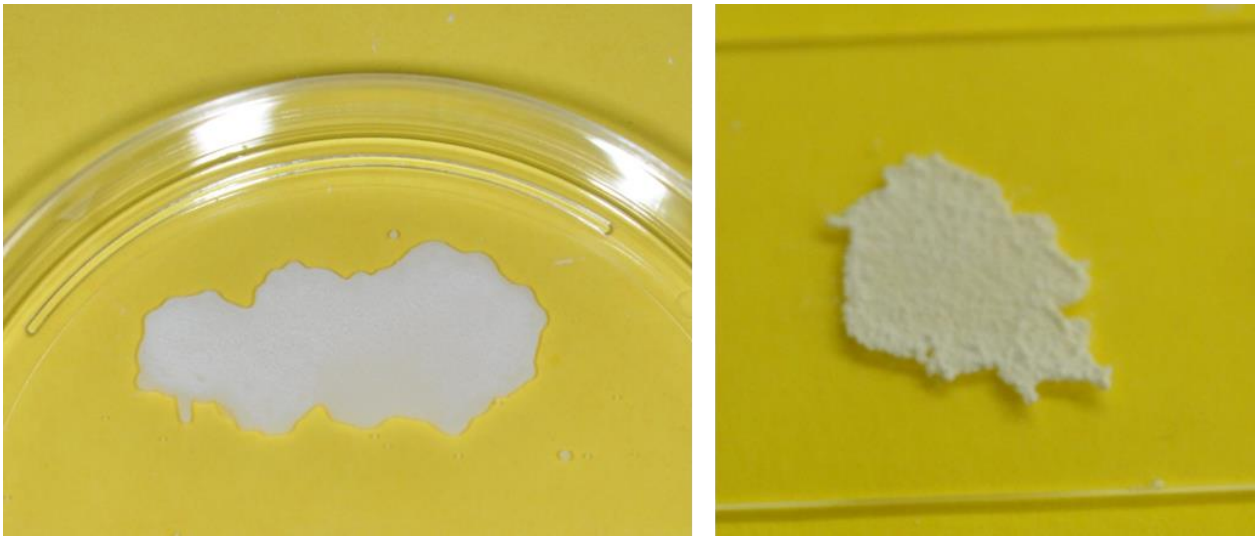

Figure 19 ODTS films assembled on polypropylene (left) and a glass microscope slide (right)

With the assembly demonstrated on glass, this substrate was selected as the primary focus for further experimentation. The next point that seemed necessary to address was whether this type of polymerized film morphology was unique to ODTS polymerized in this manner or if the entire family of n-alkyltrichlorosilanes would behave similarly. Films were prepared using the same methodology for a series of n-alkyltrichlorosilanes with various alkyl chain lengths (n = 8, 10, 12, 16, 18, and 22). The films are shown in Figure 20 below. They show that this polymerization result is not unique to ODTS, but is rather characteristic of the alkyltrichlorosilane family generally.

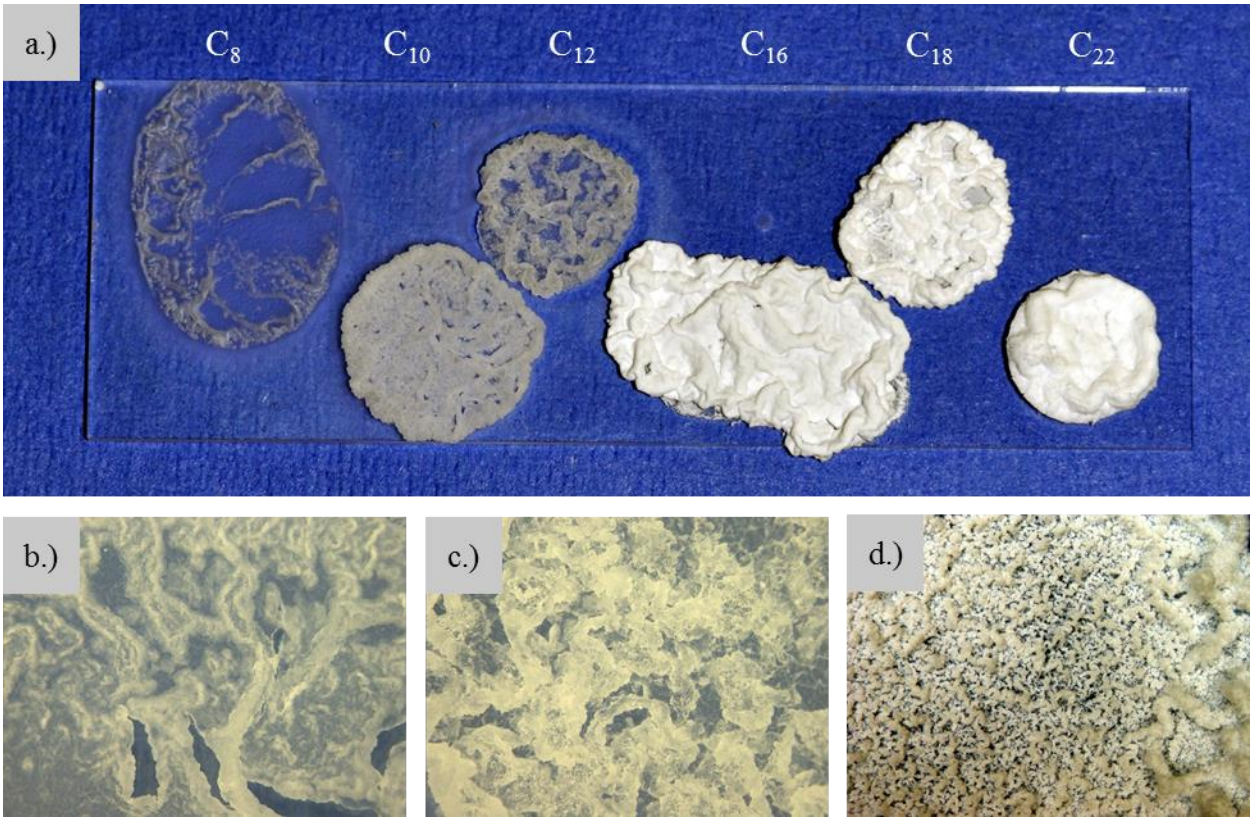

Figure 20 a) Vertically polymerized n-alkyltrichlorosilane films with differing alkyl chain lengths. Optical microscopic images of selected poly(n-alkyl)siloxane films with n = 8 (b), 12 (c), and 18 (d).

The morphology of the resultant films is clearly impacted by the alkyl chain length, with the films becoming rougher and a more opaque white as the number of carbons is increased. The alkyltrichlorosilanes with shorter chain length give a flakier, more fragile film. Additionally, the chain length has a significant effect on the kinetics of the polymerization. Octyltrichlorosilane (n = 8) was seen to react completely after ~ 2 h, whereas docosyltrichlorosilane (n = 22) required approximately 3 days to polymerize to its final form. Hexadecyl- and octadecyltrichlorosilane offered the most desirable architectures for reproduction by μMSIP, and ODTS was selected for further experimentation because of the greater availability of characterization for ODTS mono- and multilayers in the literature[21,22].

We have successfully produced these rough films on silica, polypropylene, and poly(2-octyl)acrylate (commercial tape). It was initially assumed that the reaction was contingent on the presence of surface hydroxyl groups considering their role in monolayer formation – however, the success of this polymerization on polypropylene suggests otherwise. Several key factors were examined as relevant parameters, including water content at the surface and the method by which the water was applied, the effect of surface hydroxylation of silica substrates using piranha solution, reaction time and temperature, and the effect of diluting the ODTS in a solvent such as DCM. These aspects of the procedure were analyzed to optimize the film properties for replication with μMSIP.

Water is known to play an indispensable role in catalyzing the polymerization of trichlorosilanes and was therefore expected to be one of the most important parameters in controlling this process. The properties of the final ODTS films vary substantially with the amount and distribution of water on the surface. One essential feature of these ODTS films is that they must remain firmly bound to their substrate because weak attachment could lead to the

film being removed from the surface during the micromolding step. Water appears to play a critical role in this facet of the process for reasons that are somewhat unclear. When ODTS is vertically polymerized on a dry silica surface, for instance, several things happen. First, the reaction time is elevated significantly because the primary catalyst is present only in trace amounts on the surface or in the atmosphere under which the reaction occurs. Further, the spreading of ODTS droplets on the surface is reduced and a reactive front at the contact line results in the sporadic movement of the drop over the surface, causing irregularities in the structure. These films tend to be fluffier in appearance, and a majority of the polymerized material is easily knocked from the surface by the slightest force.

ODTS is traditionally adsorbed onto surfaces from a solution, and therefore, we sought to examine the effect that dilution of ODTS with a solvent might have on the ultimate film produced by the polymerization. DCM was chosen as the solvent for practical reasons, because it is used extensively throughout the μMSIP process. Additionally, the low boiling point of DCM was of interest as it was expected to evaporate away for the final product. In Figure 21 below, comparisons of films grown with pure ODTS (left) and 10% ODTS in DCM (right) are shown, with all other synthesis parameters kept identical.

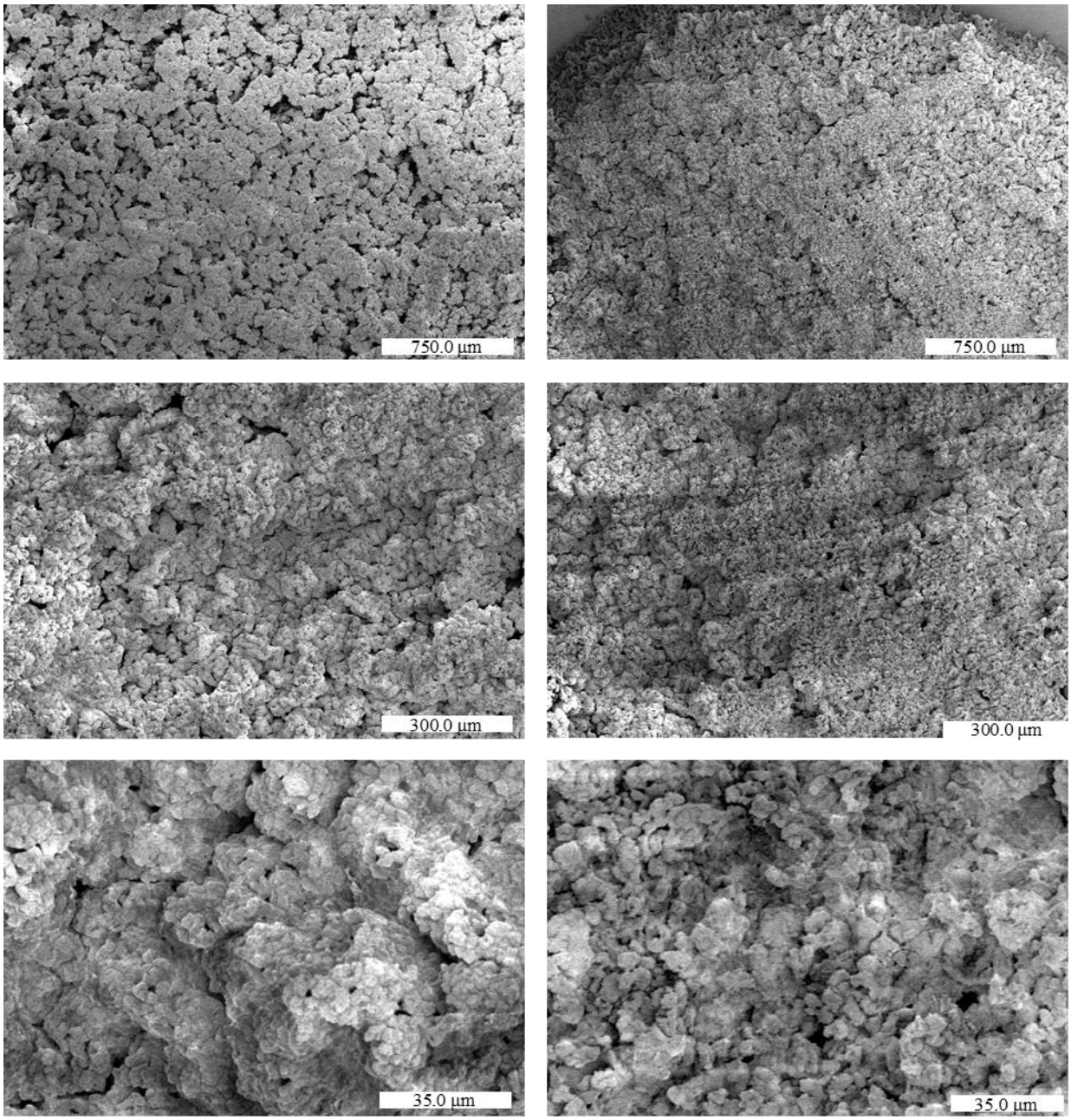

Figure 21 n-Octadecyltrichlorosilane films grown on silica with pure ODTS (left) and 10% ODTS in DCM (right). While the films appear similar at larger scales, smaller, more particulate features seem to comprise the film grown with 10% ODTS in DCM

The above images suggest that while the films appear identical at larger magnifications, closer inspection shows that the films grown with DCM as solvent have a rougher architecture

comprised of smaller particulates. These would be expected to give a higher contact angle because of the more pronounced re-entrance and greater number of pockets for trapped air. Additionally, the films prepared with DCM as solvent are more uniform, much less thick, and less likely to flake from the surface. All of these are valuable for our purposes.

Films were also prepared to evaluate the usefulness of surface hydroxylation of silica substrates with piranha solution prior to addition of the ODTS. The mentality underlying this rests on the fact that conventional wisdom for this reaction holds that the trichlorosilanes attach to the surface via exposed hydroxyl groups. If the density of hydroxyl groups is increased at the surface, it is possible that greater chemical attachment could occur. To test this, films of both pure ODTS and 10% ODTS in DCM were prepared using each of the water delivery methods and half used a silica substrate treated by piranha while half did not. It was found that the piranha treatment conferred no significant improvements for wetted samples, and therefore this step was generally omitted. Barring evidence of a strong justification for its use, this step can be omitted for films to be used for micromolding. It simply adds time and requires use of a highly dangerous material with little benefit ultimately gained.

Another consideration in ensuring faithful casting of any surface, we must consider the surface energies of the materials involved. At its simplest, a mold that has cured will be more readily peeled from a substrate as the surface energy of that substrate is reduced. While the surface of the octadecyltrichlorosilane polymer is comprised predominantly of aliphatic chains – among the lowest energy surfaces available – the surface could be made still lower energy by incorporating fluorinated groups at the surface. Because it is clear that trichlorosilanes react readily with themselves, it was expected that treatment of an ODTS surface with another trichlorosilane having a fluorinated chain would yield a lower energy surface. Tridecafluoro-

1,1,2,2,-tetrahydrooctyl)-1-trichlorosilane (TFOCS) is used frequently to reduce the energy of a surface (silica, for instance) as part of its preparation for molding. TFOCS was therefore chosen as a candidate material for imbuing these ODTS polymer surfaces with fluorocarbon like properties.

Typically, TFOCS is applied to a substrate in the vapor phase by placing the surface and a small quantity (i.e. a drop) of the trichlorosilane under vacuum for 30 min. This approach was used to treat both a surface-bound ODTS polymer film and a quantity of the bulk ODTS polymer. FTIR was used to demonstrate the success of the reaction. FTIR spectra are shown from before and after TFOCS treatment in Figure 22 below. The peak at 1237 cm^{-1} in the lower spectrum indicates the presence of the C-F bonds, suggesting successful adsorption of the TFOCS to the exterior surface of the ODTS polymer.

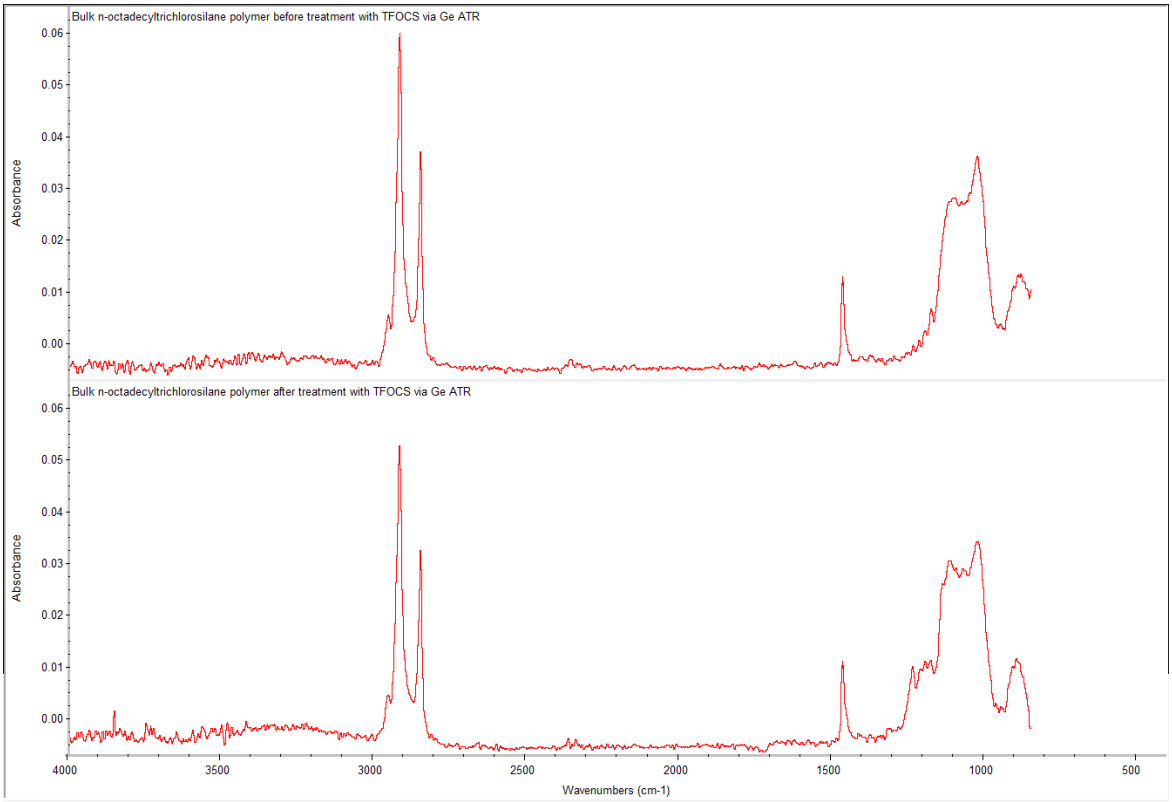

Figure 22 ATR-FTIR measurements of the octadecyltrichlorosilane polymer before and after treatment with TFOCS indicate the successful adsorption of the fluoroalkyltrichlorosilane, due to the peak present at 1237 cm^{-1}

Further, contact angle measurements were taken before and after the TFOCS treatment, and these showed a non-negligible increase in both the advancing and receding contact angles, corroborating the results from FTIR. Before treatment, θ_a/θ_r for the ODTS films is 164º/161º, whereas after treatment this is elevated to 172º/170º.

3.6 Reproduction of Poly(n-octadecyl)siloxane Films with μMSIP

Thin films based on octadecyltrichlorosilane have a variety of morphologies depending rather sensitively on the particular conditions of the polymerization, especially the water content

and distribution, the use of solvent, and temperature. SEM was performed on films having a variety of architectures, and a sampling of these is shown in Figure 23 below.

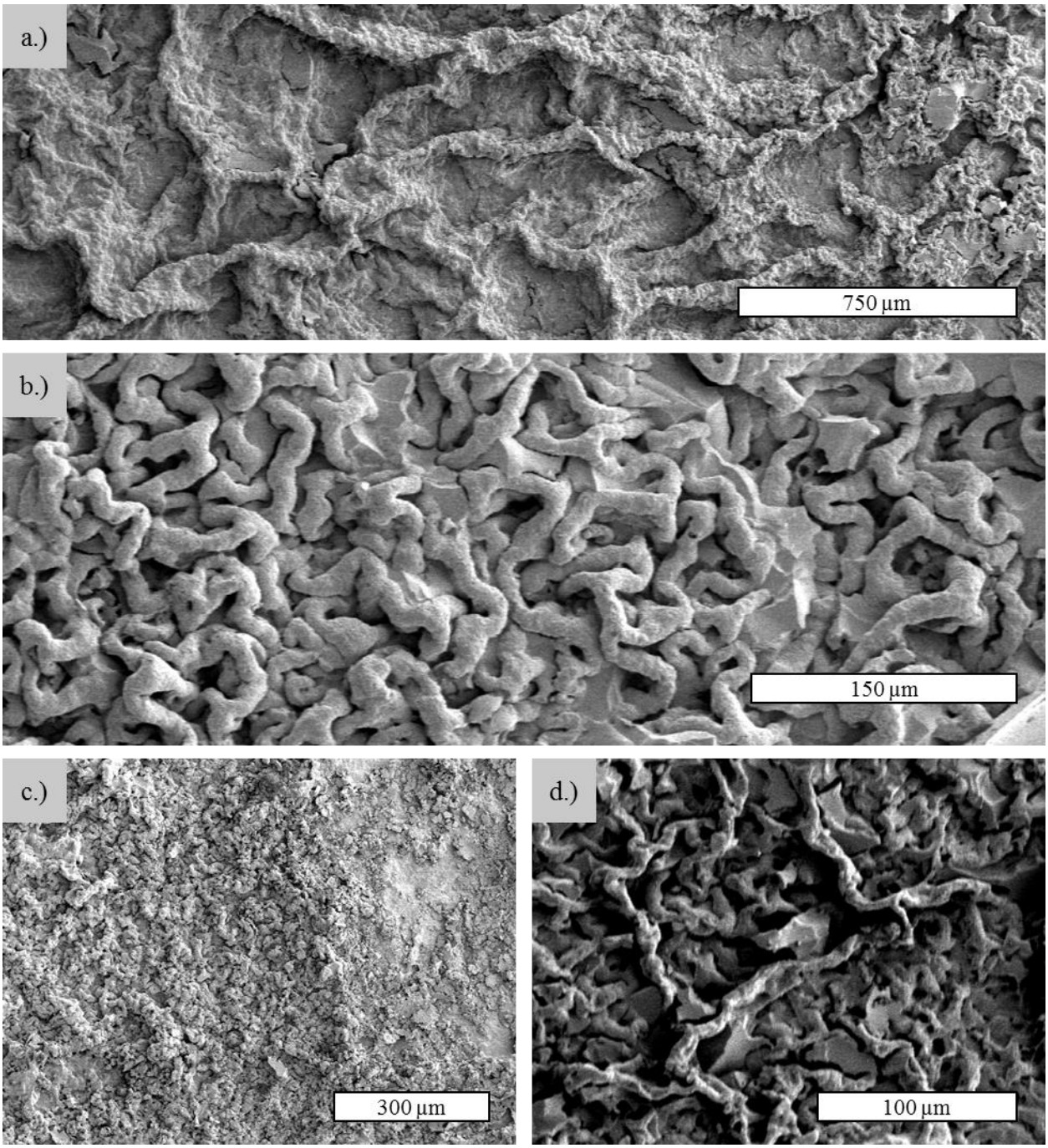

Figure 23 Scanning electron microscopic images PNBF8 film reproductions formed via µMSIP and based on a variety of vertically polymerized ODTS films on glass

The above films were fabricated using µMSIP and show the success of extending this approach to more complex architectures than those demonstrated previously. The surfaces show

re-entrance and hierarchical roughness with features both larger and smaller than any of those on surfaces from previous work, emphasizing that this technique has application over a wide range of feature sizes. As a consequence of the re-entrance and hierarchical roughness combined with the ultralow surface energy of these interfaces, they show significant repellency toward both water and oils. Despite the differing morphologies of the films, the contact angle measurements were similar for these films, and average values for these are presented in Table 3 below for all films bearing the fibril-like architectures seen in Figure 23 a), b), and d).

Table 3 Summary of average water and hexadecane contact angles for PNBF8 films based on vertically polymerized ODTS masters

Probe Fluid	θ_a	θ_r
Water	172º ± 2º	168º ± 2º
Hexadecane	154º ± 2º	150º ± 1º

The key to these high contact angles is the re-entrant geometry and the hierarchical feature size. While the largest structures can be hundreds of microns in size, they are comprised of many smaller constituents tens of microns and smaller, as shown in Figure 24 below.

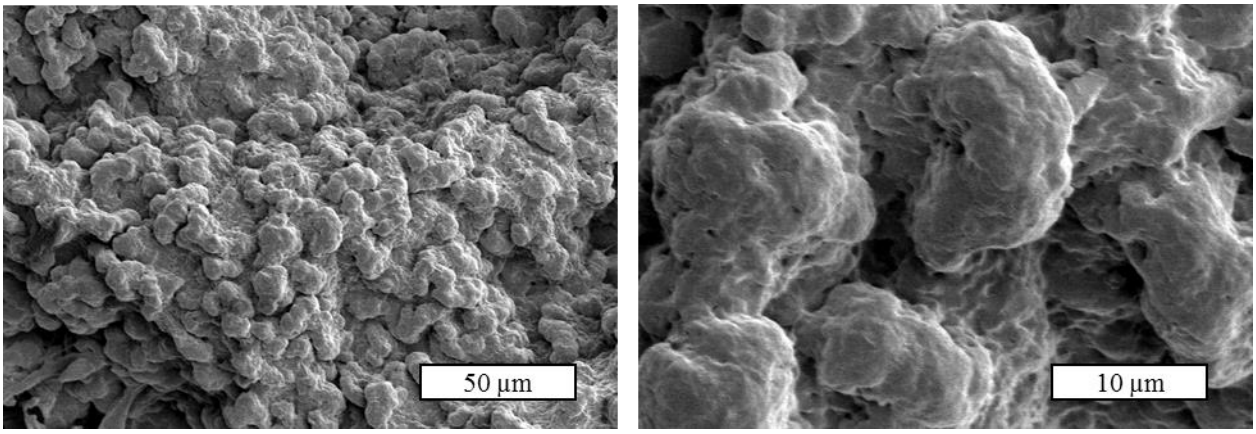

Figure 24 SEM images of PNBF8 films show features with sizes tens of microns and smaller. The above are higher magnification images of the film shown in Figure 23a.

Even submicron features were able to be replicated using µMSIP and the hard PDMS molding procedure, for example those seen in Figure 25 below.

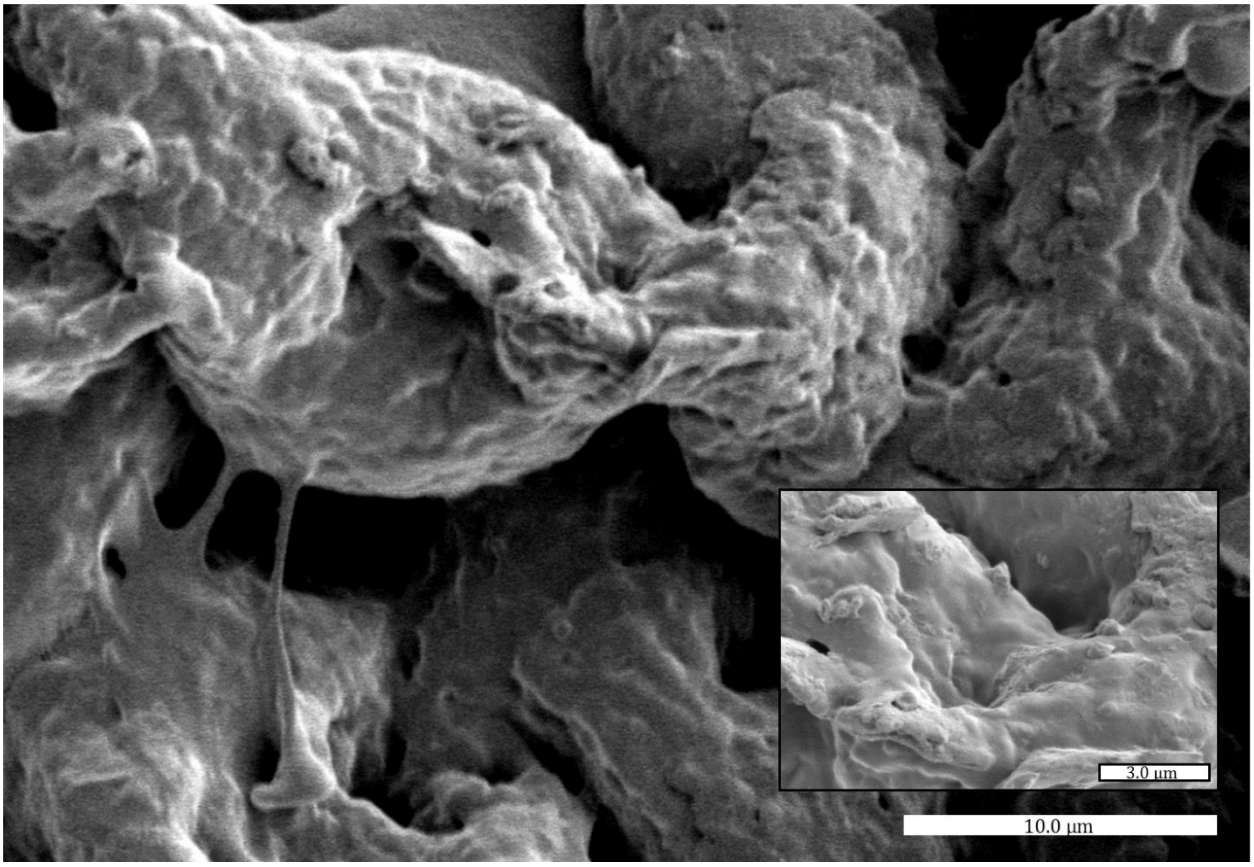

Figure 25 SEM images of PNBF8 films fabricated with micromolding surface-initiated polymerization show features microns in size and smaller

Because the interest in fabricating the vertically polymerized surfaces rests on the possibility of modulating the surface features to ones needs, it is worth noting that another way to control the morphology of the films is to wash the ODTS master surface with water and ethanol at some time before the polymerization is allowed to proceed to completion. This has the effect of eliminating much of the smaller scale structuration leading to a smoother surface but still bearing resemblance to the films seen above in terms of the larger architecture. Such a film can be seen in Figure 26 below.

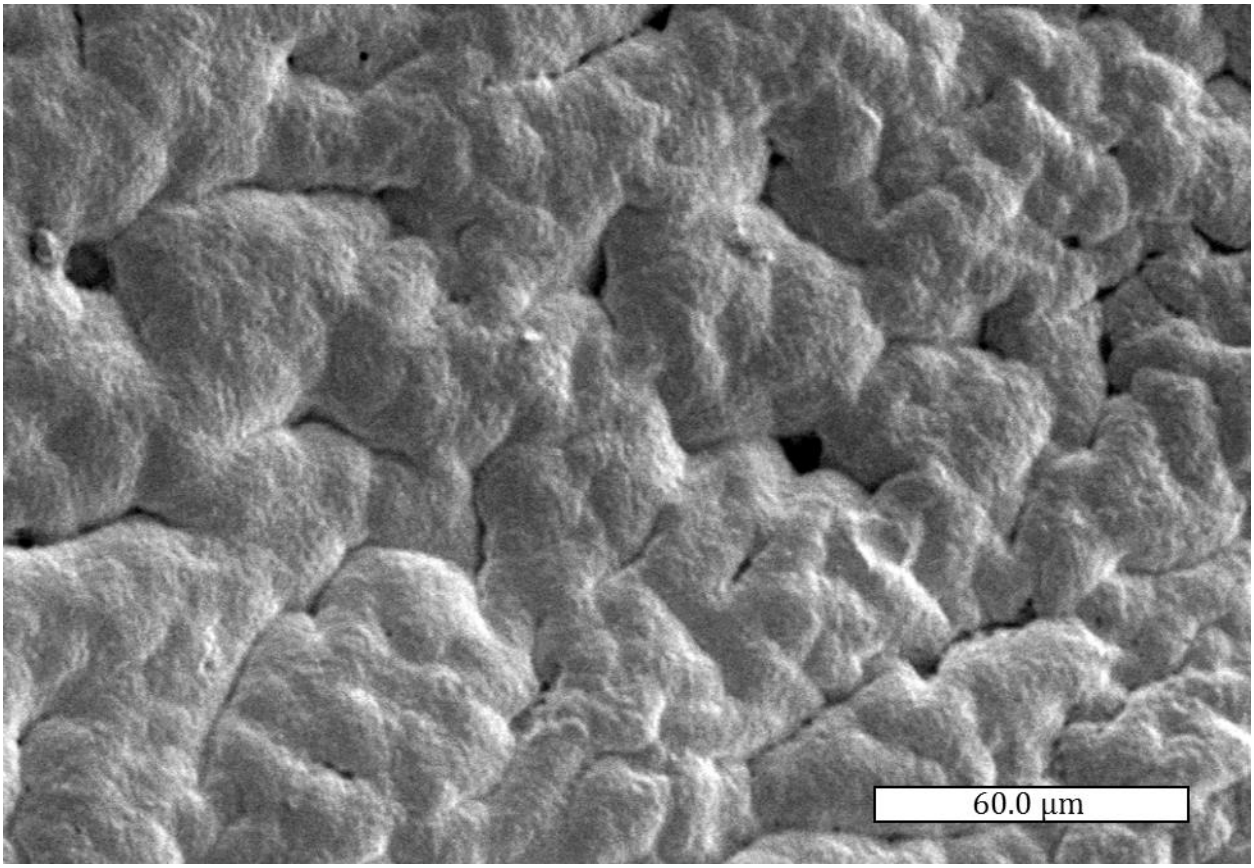

Figure 26 SEM image of a PNBF8 film fabricated via micromolding surface-initiated polymerization with a mold based on an ODTS film on glass that was washed before the polymerization could proceed to completion.

On a final note, a problem introduced by the re-entrant geometry of these surfaces is that the micromolding polymer (hPDMS in this case) may become trapped in the recesses of the fluoropolymer surface after the SIP step has been performed and may break off during the mold removal step. This results in hPDMS stuck in crevices of the PNBF8 film that cannot easily be removed. This can be seen in the PNBF8 films shown in Figure 27 below.

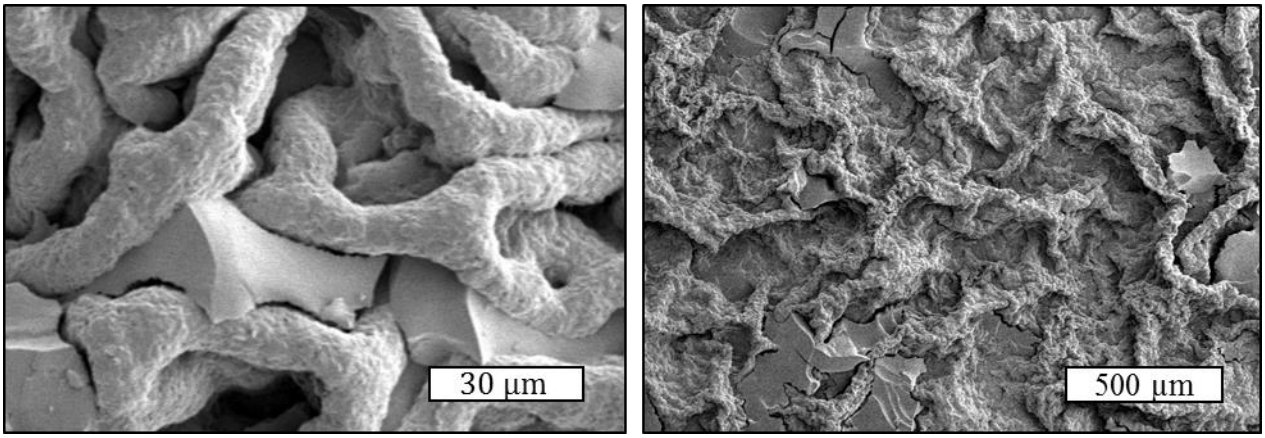

Figure 27 SEM images of PNBF8 films show hPDMS trapped in the recesses of the film due to break-off as the mold was removed

This trapped hPDMS has a number of negative consequences and represents a problem relevant to any molding procedure involving surfaces with re-entrant geometries. First, it means that the mold is degraded with each use. One of the advantages of molding a surface is that ideally the mold can be used repeatedly to reproduce the master surface, greatly improving the efficiency especially compared to photolithographic techniques. If damage to the mold limits its use to one or several times, one of the most alluring aspects of this approach is diminished. Second, trapped hPDMS also means that the PNBF8 composition no longer possesses a uniform fluorocarbon composition and is contaminated with aliphatic and siloxane groups. This leads to a reduction in the advancing and receding contact angles due to the increased surface energy of these regions. The magnitude of the reduction is increased as the quantity of trapped hPDMS becomes larger. This contamination can also lead to contact line pinning and increased hysteresis.

4 Conclusions & Future Work

4.1 Conclusions

Micromolding surface-initiated polymerization has proven itself an exciting and versatile addition to the soft lithographic toolbox. This approach offers a variety of unique characteristics, most notably the chemical attachment of the polymer film to its substrate and the relatively simple route to partially fluorinated polymer films. The potential for variation on its fundamental concepts is infinite. It seems almost any surface conceivable has potential for successful reproduction; gold could be replaced by any other material as the substrate for SIP as long as proper chemistry was employed to activate the surface. Other polymers shown to undergo surface-initiated polymerizations could be used in place of the PNBF8 used for this work. Because of that, the objectives of this work were necessarily broad and focused on advancing the technique beyond what has been demonstrated previously with the hope of promoting its further use.

Novel surfaces were fabricated for reproduction using techniques not described in the literature. Films of vertically polymerized n-octadecyltrichlorosilane were synthesized on a variety of substrates, including silica, polypropylene, and poly(2-octyl)acrylate. This process results in dramatic roughness at both the micro and nanoscales, offering strong water repellency properties. Superhydrophobicity of the unmodified films was demonstrated, as was the feasibility of elevating the contact angle further by treatment of the ODTS polymer with a fluoroalkyltrichlorosilane. This resulted in advancing contact angles in excess of 170º and with low hysteresis (< 5º). Various reaction parameters – including the influence of water on the surface, the effect of surface hydroxylation, and the effect of solvent – were analyzed to optimize

the ODTS films for reproduction with μMSIP. We found that water applied to the surface via a brief (~1 s) exposure of the cleaned substrate to saturated steam at atmospheric pressure resulted in superior films when compared to dry substrates or substrates wetted with a stream from a wash bottle. Treatment of the silica surfaces with piranha solution offered no obvious benefit, and given the hazardous nature of this material, it is better omitted until its importance is shown. Reactions carried out with a 10 % ODTS in DCM solution led to films with similar morphologies to those of pure ODTS when viewed at the microscale; however, in the nano realm, the 10 % solution results in smaller particulates comprising the architecture as well as an increase in the volume of air pockets.

Substrates based on copper foils having undergone an aqueous ammonia etching procedure were also investigated. It was found that at etching times of ~ 24 h, the process formed black CuO films at the surface with grains tens of microns in size covered in nanohairs < 100 nm in length and ~ 10 nm in diameter. At longer etching times, allowing for complete evaporation of the etching solution, this black CuO surface was replaced by a bright blue patina composed of a network of fused copper (I) hydroxide nanoparticles ~ 300 nm in diameter. Both surfaces were modified by adsorption of n-octadecanethiol, and the success of the reaction was shown by ATR-FTIR. After modification, the black CuO and the blue patina surfaces displayed advancing water contact angles of $150^{o} \pm 4^{o}$ and $162^{o} \pm 3^{o}$, respectively. The high water repellency suggested these surfaces would be useful candidate substrates for μMSIP.

With new approaches for substrate fabrication, μMSIP was extended to more difficult surfaces to reproduce than those previously demonstrated. Successful reproduction of both re-entrant surface architectures as well as micro- and nanoscale roughness was accomplished, representing a significant and valuable advancement for this technique as both are requirements

for superantiwetting surfaces. Higher water contact angles and more robust superhydrophobicity was demonstrated for films based on vertically polymerized ODTS masters than had been seen for any of the surfaces molded previously. Superoleophobicity was also achieved, with and advancing hexadecane contact angles of 154 º± 2º and a receding of 151º ± 2º.

4.2 Future Work

With μMSIP extended to smaller architectures and re-entrant surfaces, the value of this technique is unmistakable, and tremendous potential for future research exists. Countless incarnations of this approach are waiting to be explored, and much room for improvement exists even for the substrates already examined. This family of soft lithographic approaches offers the engineer a chance to tune surface architecture to meet whatever needs exist. The research presented here represents only a tiny fraction of what one can do under the umbrella of micromolding surface-initiated polymerization. The partially fluorinated polymers presented are only one possibility, and any other polymer that can undergo surface-initiated polymerization could be used instead.

Gold is used as a substrate here for the well-understood chemistry involved, but any other surface could be used with appropriate modification to the attachment chemistry and activation approach. Copper would be a strong next candidate for research, as the same activation approach as presented here would likely also be viable because of the similar affinity of thiols for forming monolayers on copper surfaces.

As for improving on the current work, the biggest challenge to reproduction of re-entrant surfaces is the pieces of the mold may become lodged in recesses of the mold and break off as the mold is removed. This leads to damage to the mold and a reduction of the desirable

properties of the film. Mitigating this problem can be approached in several ways. First, the exact composition of the hPDMS used can be adjusted to reduce the brittleness or fragility of small features so that they are likely to break off. Additionally, reducing the attraction of the hPDMS mold to the resultant surface can be achieved by fluorinating the interior of the mold with the same approach described for fluorinating the poly(n-octadecyl)siloxane surfaces (vapor-phase treatment with TFOCS). This leads to a reduction of the surface energy of the mold exposed to the final polymer films, which also reduces the attractive force of the mold to the surface, making the removal process less likely to result in fracture.

Regardless, micromolding surface-initiated polymerization has demonstrated its role as an effective way to reproduce surface architectures with elaborate and even re-entrant structuration. Interest in surfaces is unlikely to diminish in coming years with so many unanswered questions surrounding them. Application of polymer films to surfaces has already demonstrated its commercial importance, with no better example than Teflon cookware, but the existing approaches all rely on physical attachment to surfaces. By combining robust chemical attachment with the ability to tune surface architecture to almost any structure imaginable, micromolding surface-initiated polymerization represents an unparalleled tool not only for academic investigation but also in commercial applications yet to be envisaged.

References

1. Garbassi, F., Morra, M. & Occhiello, E. *Polymer Surfaces: From Physics to Technology*. (Wiley, 1997).
2. Shaw, D. *Introduction to Colloid and Surface Chemistry, Fourth Edition*. (Butterworth-Heinemann, 1992).
3. Hounshell, D. A. *Science and Corporate Strategy: Du Pont R and D, 1902-1980*. (Cambridge University Press, 1988).
4. Ebnesajjad, S. *Introduction to Fluoropolymers: Materials, Technology and Applications*. (William Andrew, 2013).
5. Faulkner, C. J., Fischer, R. E. & Jennings, G. K. Surface-Initiated Polymerization of 5-(Perfluoro-n-alkyl)norbornenes from Gold Substrates. *Macromolecules* **43,** 1203–1209 (2010).
6. Brantley, E. L. & Jennings, G. K. Fluorinated Polymer Films from Acylation of ATRP Surface-Initiated Poly(hydroxyethyl methacrylate). *Macromolecules* **37,** 1476–1483 (2004).
7. Kim, J.-B., Huang, W., Bruening, M. L. & Baker, G. L. Synthesis of Triblock Copolymer Brushes by Surface-Initiated Atom Transfer Radical Polymerization. *Macromolecules* **35,** 5410–5416 (2002).
8. Matyjaszewski, K. *et al.* Polymers at Interfaces: Using Atom Transfer Radical Polymerization in the Controlled Growth of Homopolymers and Block Copolymers from Silicon Surfaces in the Absence of Untethered Sacrificial Initiator. *Macromolecules* **32,** 8716–8724 (1999).
9. Berron, B. J., Graybill, E. P. & Jennings, G. K. Growth and Structure of Surface-Initiated Poly(n-alkylnorbornene) Films. *Langmuir* **23,** 11651–11655 (2007).

10. Perez, E., Laval, J. P., Bon, M., Rico, I. & Lattes, A. Synthesis of bicyclo [2· 2· 1] hept-2-enes with mono and disubstituted long perfluorinated chains CnF2n+1 (n = 4,6,8,10) Investigation of association in solution by 19F NMR study of polymerization via a metathetic reaction. *J. Fluor. Chem.* **39,** 173–196 (1988).
11. Del Campo, A. & Arzt, E. Fabrication Approaches for Generating Complex Micro- and Nanopatterns on Polymeric Surfaces. *Chem. Rev.* **108,** 911–945 (2008).
12. Xia, Y. *et al.* Complex Optical Surfaces Formed by Replica Molding Against Elastomeric Masters. *Science* **273,** 347–349 (1996).
13. Bixler, G. D. & Bhushan, B. Bioinspired rice leaf and butterfly wing surface structures combining shark skin and lotus effects. *Soft Matter* **8,** 11271–11284 (2012).
14. Tuteja, A. *et al.* Designing Superoleophobic Surfaces. *Science* **318,** 1618–1622 (2007).
15. Escobar, C. A., Cooksey, T. J., Spellings, M. P. & Jennings, G. K. Micromolding Surface-Initiated Polymerization: A Versatile Route for Fabrication of Coatings with Microscale Surface Features of Tunable Height. *Adv. Mater. Interfaces* **1,** n/a–n/a (2014).
16. Jennings, G. K. & Brantley, E. L. Physicochemical Properties of Surface-Initiated Polymer Films in the Modification and Processing of Materials. *Adv. Mater.* **16,** 1983–1994 (2004).
17. Escobar, C. A., Spellings, M. P., Cooksey, T. J. & Jennings, G. K. Reproducing Superhydrophobic Leaves as Coatings by Micromolding Surface-Initiated Polymerization. *Macromol. Rapid Commun.* n/a–n/a (2014). doi:10.1002/marc.201400412
18. Ulman, A. in *Kirk-Othmer Encyclopedia of Chemical Technology* (John Wiley & Sons, Inc., 2000). at <http://onlinelibrary.wiley.com.proxy.library.vanderbilt.edu/doi/10.1002/0471238961.1315141521121301.a01/abstract>

19. Fadeev, A. Y. & McCarthy, T. J. Self-Assembly Is Not the Only Reaction Possible between Alkyltrichlorosilanes and Surfaces: Monomolecular and Oligomeric Covalently Attached Layers of Dichloro- and Trichloroalkylsilanes on Silicon. *Langmuir* **16,** 7268–7274 (2000).
20. Liu, X. *et al.* Clam's Shell Inspired High-Energy Inorganic Coatings with Underwater Low Adhesive Superoleophobicity. *Adv. Mater.* **24,** 3401–3405 (2012).
21. Parikh, A. N. *et al.* n-Alkylsiloxanes: From Single Monolayers to Layered Crystals. The Formation of Crystalline Polymers from the Hydrolysis of n-Octadecyltrichlorosilane. *J. Am. Chem. Soc.* **119,** 3135–3143 (1997).
22. Wasserman, S. R., Tao, Y. T. & Whitesides, G. M. Structure and reactivity of alkylsiloxane monolayers formed by reaction of alkyltrichlorosilanes on silicon substrates. *Langmuir* **5,** 1074–1087 (1989).